Lithos 202–203 (2014) 85–99

Contents lists available at ScienceDirect

Lithos

journal homepage: www.elsevier.com/locate/lithos

Petrogenesis of a Late Carboniferous mafic dike–granitoid association in the western Tianshan: Response to the geodynamics of oceanic subduction

Gong-Jian Tang [a,b,*], Sun-Lin Chung [b], Qiang Wang [a], Derek A. Wyman [c], Wei Dan [a], Hong-Yi Chen [d], Zhen-Hua Zhao [a]

[a] State Key Laboratory of Isotope Geochemistry, Guangzhou Institute of Geochemistry, Chinese Academy of Sciences, Guangzhou 510640, Guangdong, China
[b] Department of Geosciences, National Taiwan University, Taipei, Taiwan, China
[c] School of Geosciences, The University of Sydney, NSW 2006, Australia
[d] Guangxi Key Laboratory of Hidden Metallic Ore Deposits Exploration, College of Earth Sciences, Guilin University of Technology, Guilin 541004, Guangxi, China

ARTICLE INFO

Article history:
Received 30 January 2014
Accepted 20 April 2014
Available online 2 May 2014

Keywords:
Mafic dike
Granite
Petrogenesis
Slab roll-back
Western Tianshan

ABSTRACT

Mafic dike–granitoid associations are common in extensional tectonic settings and provide important opportunities for understanding mantle and crust melting during the tectonic evolution of host orogenic belts. We report results of petrologic, whole rock geochemical, Sr–Nd isotopic data and in situ zircon U–Pb and Hf isotopes for a mafic dike–granitoid association from the Zhongyangchang pluton in the western Tianshan, in order to constrain their petrogenesis and tectonic significance. The intrusive rocks are mainly composed of granodiorite, monzogranite, and minor granitic dikes, with mafic dikes intruded into the pluton. Zircon LA-ICP-MS U–Pb ages indicate that the Zhongyangchang intrusive rocks were all emplaced during a short interval in the Late Carboniferous (317–310 Ma), establishing that the mafic and felsic magmas were coeval. The mafic rocks have low SiO_2 and high MgO concentrations, with low $^{87}Sr/^{86}Sr$ ratios from 0.7048 to 0.7053 and positive $\varepsilon_{Nd}(t)$ and zircon $\varepsilon_{Hf}(t)$ values from +2.9 to +3.8 and +12.2 to +13.6, respectively. They are enriched in large ion lithophile elements (LILEs) and depleted in high field strength elements (HFSEs), which can be explained by an origin from melting of a depleted lithospheric mantle source and source fluxing by fluids derived from the down-going slab. Granitoids from the pluton have high SiO_2 contents and low MgO concentrations, suggesting that they were mainly derived from crustal sources. They also have positive whole rock $\varepsilon_{Nd}(t)$ and zircon $\varepsilon_{Hf}(t)$ values ranging from +0.2 to +2.8 and +6.6 to +15.3, respectively, similar to those of the mafic dikes. They were generated by partial melting of juvenile basaltic lower crust as a result of magma underplating. The Late Carboniferous mafic dike–granitoid association was not related to a post-collisional setting, but rather formed in an arc environment related to oceanic subduction. The most likely tectonic model accounting for the genesis of these rocks involves an extensional environment in the western Tianshan during the Late Carboniferous as a tectonic response to the roll-back of subducted Junggar oceanic lithosphere, which could also account for the "flare-up" of Late Carboniferous magmatism.

1. Introduction

Mafic dike–granitoid associations are common in extensional tectonic settings and provide important opportunities for understanding the sources of mantle magmas, crust–mantle interaction processes, crustal melting, and the tectonic evolution of orogenic belts. It is generally accepted that mafic dike–granite associations were emplaced in extensional tectonic regimes linked to post-collisional or intraplate extensional settings (Eby, 1992; Said and Kerrich, 2010; Xu et al., 2008; Yang et al., 2007b). However, the genetic relationship between granites and mafic rocks is a matter of much current debate. Three very different processes proposed for the generation of granites include: (1) fractional crystallization of parental basic melts of mantle-derived magmas with a range of pressures and compositions; (2) partial melting (anatexis) of pre-existing lower crust mafic sources such as basaltic rocks or amphibolites, or a protolith of hornblende-rich diorite to granodiorite in the mid- to upper crust; (3) mixing between mafic and felsic magmas derived from mantle and crustal sources, respectively, where mafic dikes represent the mafic magma.

The Tianshan Orogen extends from west to east for over 2400 km through Uzbekistan, Tajikistan, Kyrgyzstan, and Kazakhstan to Xinjiang in northwestern China and developed by multiple subduction events in the Junggar–Balkhash and South Tianshan Oceans (Paleo-Asian Ocean) for the north and south parts of Tianshan, respectively (Charvet et al., 2011; Gao et al., 2009; Xiao et al., 2010, 2013) (Fig. 1a). An extensive

* Corresponding author at: State Key Laboratory of Isotope Geochemistry, Guangzhou Institute of Geochemistry, Chinese Academy of Science, Guangzhou, 510640.

http://dx.doi.org/10.1016/j.lithos.2014.04.010
0024-4937/

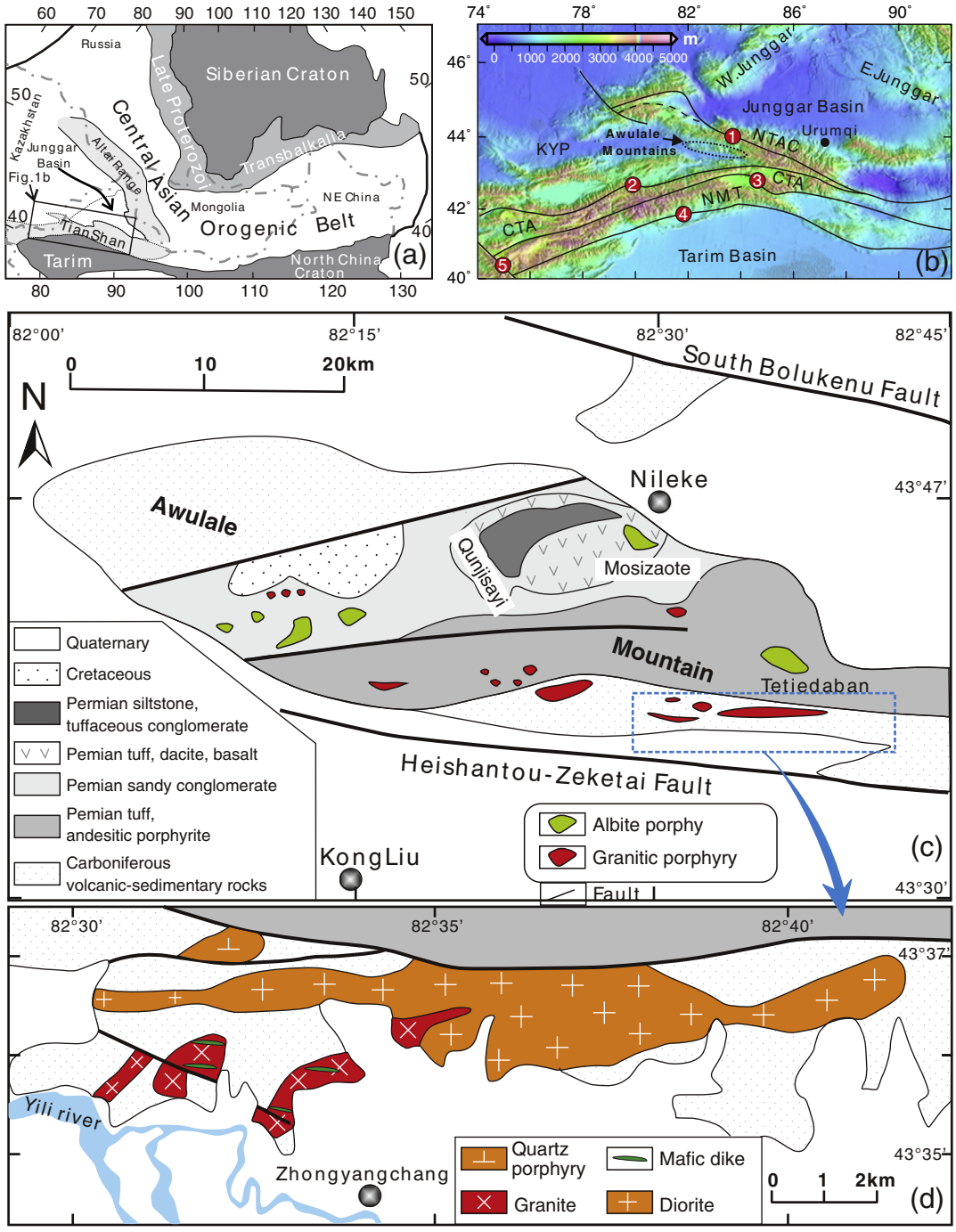

Fig. 1. (a) Tectonic sketch map of the Central Asia Orogenic Belt and the location of the Tianshan orogen (modified after Jahn et al., 2000). (b) Digital topography of the Tianshan Orogenic Belt (original data from U.S. Geological Survey [http://eros.usgs.gov/products/elevation/gtopo30.html]) showing the Awulale mountains in the core of the Tianshan, the tectonic elements are after Gao et al. (2009). (c) Geological map of the west part of the Awulale mountains (after Zhao et al., 2008). (d) Simplified geological map of the Zhongyangchang area.

belt of Paleozoic magmatic rocks was associated with subduction of oceanic lithosphere beneath continental lithosphere, corresponding to a major part of the southwestern Central Asian Orogenic Belt (CAOB) (Jahn et al., 2000; Xiao et al., 2004, 2013; Windley et al., 2007; Gao et al., 2011). There is a debate, however, on the timing of final closure of the Junggar Ocean, with estimates ranging from Early Carboniferous to Late Permian (Allen et al., 1993; Carroll et al., 1995; Gao et al., 1998; Han et al., 2010; Tang et al., 2010; Wang et al., 2007; Xiao et al., 2008, 2013). Furthermore, the tectonic settings and magma sources of Late Carboniferous mafic and felsic rocks of the western Tianshan remain controversial, although they potentially can provide important information concerning the tectonic evolution of the Tianshan Orogen. Most research in the region has focused on the petrogenesis of Late Carboniferous granitic rocks (Long et al., 2011; Tang et al., 2010). However, little is known concerning the geodynamic and genetic relationships between the temporally and spatially related Late Carboniferous mafic and granitic rocks.

In this contribution we report new whole rock geochemical and Sr–Nd isotopic data and zircon U–Pb age and in-situ Hf isotopic compositions for a representative Late Carboniferous batholith (the Zhongyangchang batholith) in the western Tianshan, consisting of coexisting mafic dikes and granitoids, in order to constrain the sources and genetic relationship between them and to resolve the geodynamic environment at the time of emplacement.

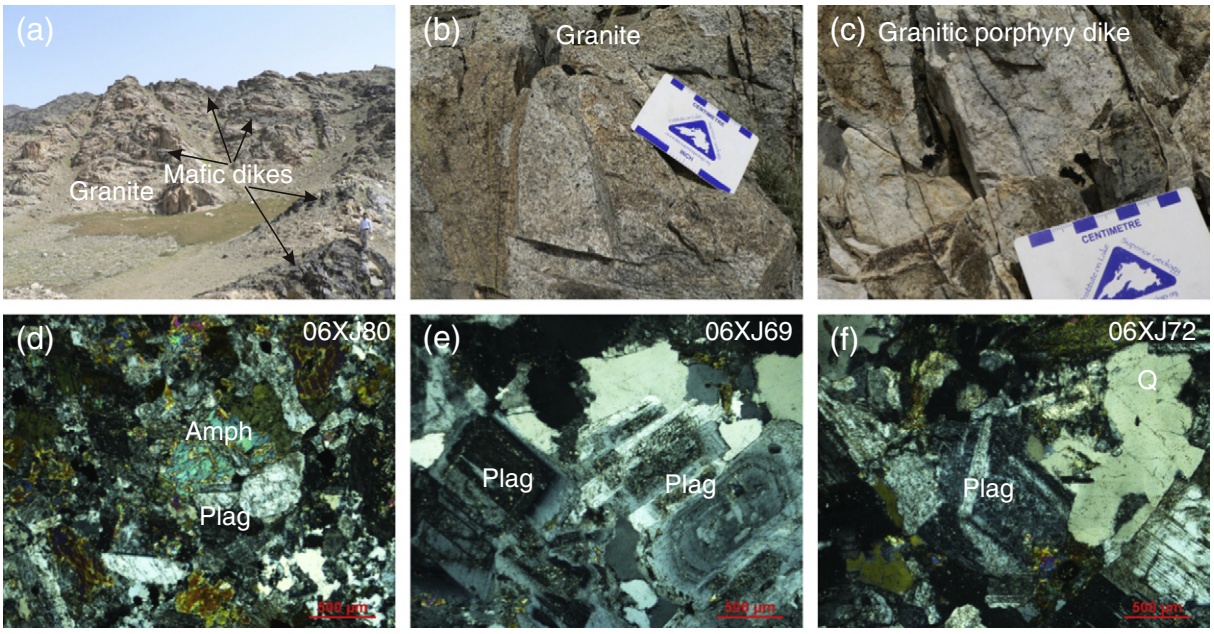

Fig. 2. Field photographs showing (a) the Zhongyangchang granitic pluton with abundance intruded mafic dikes, (b) the granite of the Zhongyangchang pluton, and (c) the sampled granitic porphyry dike occurring within Zhongyangchang pluton. Microphotographs showing (d) the amphibole and plagioclase in the mafic dike, (e) normal-zonging plagioclase in the granodiorite, and (f) amphibole and quartz in the granodiorite porphyry dike; Plag = plagioclase; Amph = amphibole.

2. Geological setting and petrography

The Chinese Tianshan, located between the Junggar plate to the north and the Tarim Block to the south, is a ca. 300 km-wide Paleozoic collisional orogenic collage (Fig. 1a). It experienced a complex evolutionary history involving Paleozoic subduction and collision, Mesozoic erosion, and Cenozoic thrusting and uplift as a consequence of the India–Eurasia collision that has continued to the present (Gao et al., 2009; Windley et al., 1990; Xiao et al., 2013). The west part of Chinese Tianshan is subdivided into the north and south domains that are separated by the Kazakhstan–Yili Block, which is a microcontinent with a Precambrian basement (Allen

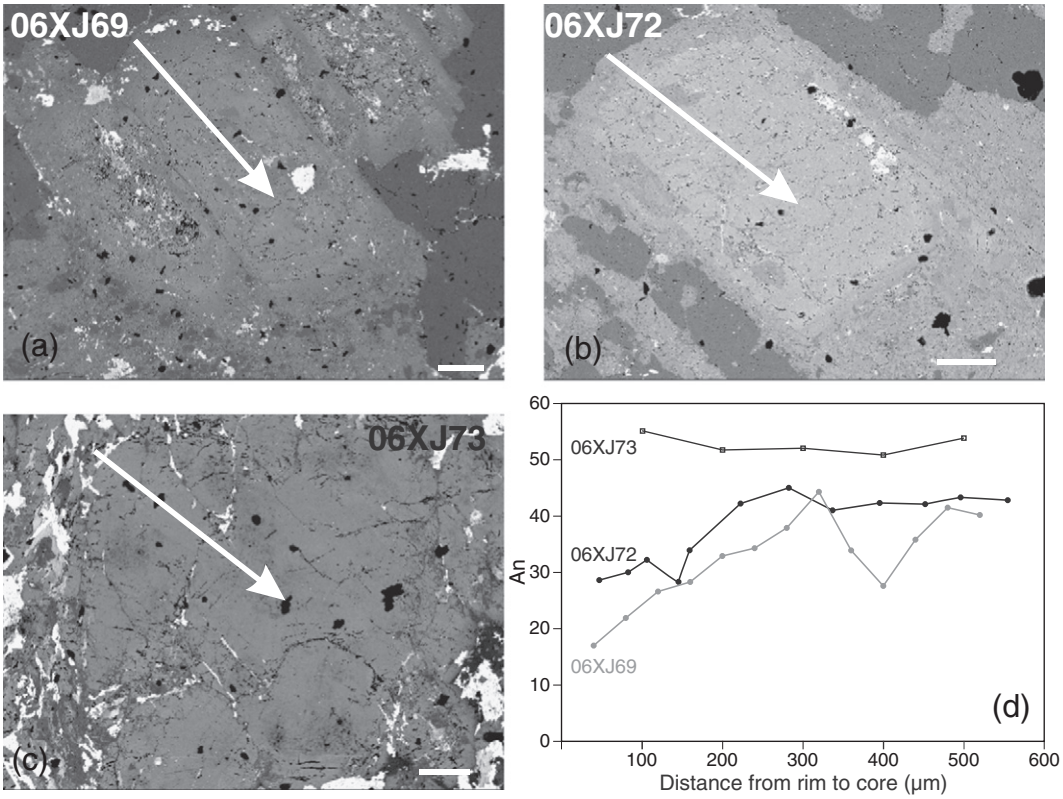

Fig. 3. Back-scattered electron images of representative phenocrysts found in the Zhongyangchang granodiorite (a), granodiorite dike (b) and mafic dike (c). Scale bars represent 100 μm. (d) Variation in plagioclase X_{An} from rim to core.

Table 1
Major (wt.%) and trace elements (ppm) and Sr–Nd isotope compositions of the rocks from the Zhongyangchang pluton.

Sample	06XJ68	06XJ70	06XJ73	06XJ76	06XJ77	06XJ80	06XJ69	06XJ71	06XJ72	06XJ-79-1	06XJ-78	06XJ-74	06XJ-75
Rock type	Gabbro dike						Granitic intrusive				Granitic dike		
SiO_2	56.13	54.52	51.61	57.56	55.61	51.81	68.92	72.19	69.56	73.80	70.40	76.58	65.20
TiO_2	1.60	1.50	1.14	1.13	1.36	0.74	0.32	0.24	0.34	0.22	0.24	0.07	0.67
Al_2O_3	13.32	13.83	17.20	14.66	14.14	17.14	15.08	14.30	15.49	14.61	15.38	12.96	17.24
Fe_2O_3	13.93	13.59	11.60	11.70	12.35	10.38	3.62	2.71	2.24	1.08	2.39	1.07	1.97
MnO	0.06	0.07	0.06	0.05	0.14	0.13	0.03	0.02	0.02	0.02	0.04	0.02	0.04
MgO	2.90	3.16	3.54	2.79	3.18	5.29	1.01	0.57	1.31	0.54	0.62	0.03	1.52
CaO	5.66	6.31	8.48	5.52	6.92	8.77	4.79	2.09	6.34	7.92	3.01	3.36	8.90
Na_2O	2.76	2.62	2.76	2.75	2.95	3.27	3.35	3.38	3.63	1.55	5.08	3.21	2.68
K_2O	2.01	2.21	1.50	1.63	1.60	0.90	0.96	3.76	0.34	0.18	0.89	1.13	0.31
P_2O_5	0.18	0.09	0.09	0.11	0.18	0.03	0.03	0.01	0.03	0.04	0.01	0.00	0.22
LOI	1.15	1.67	1.74	1.68	1.04	1.23	1.50	0.88	0.77	0.53	1.45	1.10	1.57
Total	99.70	99.56	99.71	99.57	99.46	99.68	99.60	100.15	100.06	100.47	99.49	99.52	100.31
Sc	35.8	21.4	29.7	28.9	32.1	30.6	6.92	4.22	9.37	3.06	4.31	2.07	13.8
V	246	343	320	285	304	248	62.7	37.9	54.9	21.9	39.5	6.70	28.8
Cr	2.86	15.7	46.1	8.26	7.49	68.3	15.2	10.8	7.98	8.13	10.4	14.4	16.3
Co	25.4	27.3	24.0	20.9	26.2	25.2	6.11	4.31	3.60	1.47	3.77	1.19	2.47
Ni	9.06	14.0	25.3	7.58	12.4	32.1	5.49	3.22	4.81	6.13	4.70	3.34	6.25
Ga	17.1	16.6	17.2	18.1	17.0	16.2	12.6	11.8	13.0	10.4	12.4	9.40	14.9
Cs	2.25	0.72	0.23	0.95	1.90	0.63	0.99	1.04	0.31	0.30	0.21	0.44	0.42
Rb	68.9	41.9	38.8	51.5	43.4	25.0	35.6	98.1	8.19	4.90	29.4	32.3	6.87
Ba	199	340	218	227	345	209	104	706	72.9	50.4	136	166	108
Th	4.14	2.27	2.33	3.29	3.43	1.34	8.11	7.09	6.72	4.41	9.94	21.0	2.30
U	2.15	1.01	0.75	3.00	0.99	0.39	2.14	1.37	1.04	0.58	2.76	2.02	1.06
Pb	2.02	1.90	1.53	1.98	3.91	3.26	2.45	7.60	2.34	1.19	4.65	3.29	2.03
Nb	5.53	4.71	3.58	4.44	4.83	2.10	4.57	4.67	5.78	4.84	5.71	9.00	4.06
Ta	0.41	0.33	0.26	0.34	0.34	0.15	0.35	0.60	0.49	0.44	0.68	1.28	0.28
Sr	234	253	345	267	319	357	323	177	356	263	204	161	374
Y	38.3	30.3	26.5	51.1	32.1	17.0	22.2	17.8	22.7	26.1	24.0	19.6	39.1
Zr	154	140	102	128	134	60.6	138	105	89.9	122	108	119	105
Hf	4.69	4.03	3.00	3.98	3.92	1.70	4.10	3.89	3.00	3.91	3.67	5.02	3.26
La	8.27	12.5	10.8	9.72	13.0	7.18	18.5	9.50	11.6	7.69	24.8	6.82	23.7
Ce	21.7	32.1	25.6	24.0	30.1	16.7	36.7	18.3	26.2	19.5	52.3	17.1	49.9
Pr	3.56	4.53	3.68	3.66	4.38	2.35	4.53	2.12	3.25	2.45	5.73	1.86	6.59
Nd	17.4	20.9	16.5	17.2	19.3	10.6	16.5	7.65	12.8	10.1	20.1	6.90	26.6
Sm	5.41	5.30	3.99	5.50	4.98	2.63	3.43	1.70	2.83	2.70	3.77	1.78	6.05
Eu	1.22	1.21	1.01	1.22	1.26	0.81	0.79	0.57	0.56	0.31	0.70	0.09	1.15
Gd	5.93	5.75	4.24	6.45	5.22	2.69	3.39	1.90	3.03	3.05	3.72	2.14	5.78
Tb	1.14	1.03	0.76	1.34	0.94	0.49	0.62	0.40	0.56	0.63	0.61	0.41	1.07
Dy	7.07	6.28	4.65	8.45	5.84	2.96	3.73	2.81	3.55	4.12	3.83	2.77	6.61
Ho	1.47	1.32	1.00	1.88	1.21	0.65	0.81	0.63	0.79	0.93	0.80	0.62	1.41
Er	4.13	3.63	2.77	5.49	3.44	1.82	2.33	1.93	2.27	2.77	2.44	1.94	3.99
Tm	0.60	0.53	0.40	0.84	0.51	0.27	0.35	0.33	0.37	0.44	0.40	0.33	0.62
Yb	4.00	3.38	2.68	5.98	3.21	1.73	2.43	2.28	2.52	2.90	2.69	2.39	4.17
Lu	0.63	0.52	0.40	1.04	0.50	0.28	0.39	0.35	0.41	0.44	0.43	0.40	0.64
$^{87}Rb/^{86}Sr$		0.479	0.325		0.393	0.203	0.319	1.607	0.066	0.054	0.416	0.581	
$^{87}Sr/^{86}Sr$		0.707492	0.706233		0.706762	0.705774	0.706329	0.711852	0.705345	0.705799	0.706921	0.707110	
2σm		0.000014	0.000017		0.000017	0.000014	0.000016	0.000011	0.000017	0.000014	0.000016	0.000020	
$(^{87}Sr/^{86}Sr)_i$		0.7053	0.7048		0.7050	0.7049	0.7049	0.7046	0.7050	0.7056	0.7051	0.7045	
$^{147}Sm/^{144}Nd$		0.154	0.146		0.137	0.135	0.125	0.134	0.134	0.147	0.172	0.156	
$^{143}Nd/^{144}Nd$		0.512697	0.512695		0.512689	0.512702	0.512619	0.512631	0.512635	0.512681	0.152598	0.512668	
2σm		0.000005	0.000004		0.000003	0.000004	0.000003	0.000003	0.000004	0.000005	0.000003	0.000005	
$\varepsilon_{Nd}(t)$		2.9	3.2		3.4	3.8	2.5	2.4	2.5	2.8	0.2	2.2	

et al., 1993; Gao et al., 1998; Xia et al., 2004, 2008). Unambiguous crystalline Precambrian basement (~0.9 Ga) is sporadically distributed in the Tianshan orogen (Hu et al., 2010). Voluminous Late Paleozoic granitoids and volcanic rocks formed during the Late Devonian to Late Carboniferous, the latter consisting of basalt, trachyte, trachyandesite, andesite and rhyolite, occur in the Tianshan orogen. These rocks show typical subduction zone magmatism characteristics and were generated in a continental arc, induced by subduction of the Paleo-Tianshan and Paleo-Junggar Ocean (Wang et al., 2007; Zhu et al., 2009).

In the core of Tianshan Orogen, the west–east trending Awulale Mountains are located in the northeast part of the Yili block. The Paleozoic geology of the mountains is dominated by Carboniferous and Permian volcanic–sedimentary formations (Fig. 1b). The Carboniferous strata consist of sandstones, limestone and tuff, and mainly crop out in the south margin of the Awulale Mountains. Permian rocks include sandstones, breccia and intercalated basalts, andesites and dacites. Small plutons of granitoid and albite porphyry intruded into the Carboniferous–Permian formations.

The Zhongyangchang pluton, located on the southwest margin of the Awulale Mountains, intrudes into the Carboniferous volcanic–sedimentary formation. The body consists of granodiorite, monzogranite, mafic dike and minor felsic dike (Fig. 2). The mafic dikes are 0.4 m to 5 m in width and several hundred meters to several kilometers in length. They dip steeply and occur mainly in an E–W trend of 95°. They are gabbro to gabbroic diorite in composition and generally have medium-grained granular textures. The main minerals are plagioclase (~45–50 vol.%), amphibole (~40–45 vol.%), with minor clinopyroxene, biotite, epidote and Fe–Ti oxides (~5 vol.%) (Fig. 2d). Most clinopyroxene is replaced by igneous amphibole. Fe–Ti oxides mainly consist of ilmenite. Compositional zoning has not been recognized in plagioclase from the gabbro dikes, which has high An contents ranging from 34 to 55 mol% (Fig. 3, Appendix 1).

Granodiorite and monzogranite have medium- to coarse-grained texture (Fig. 2e). They are composed of plagioclase (~45–50 vol.%), alkali-feldspar (20–30 vol.%), quartz (20–25 vol.%), and amphibole (5–10 vol.%). Plagioclase shows normal-zoning (Fig. 3). Accessory minerals include apatite, zircon, titanite and Fe–Ti oxides.

Felsic dikes have granodiorite and monzogranite composition, with a medium- to fine-grained ophitic texture. The main minerals are plagioclase (45–50 vol.%), K-feldspar (10–20 vol.%), quartz (20–25 vol.%), amphibole (5–10 vol.%), and clinopyroxene (5%). Accessory minerals include Fe–Ti oxides, zircon, and apatite.

3. Analytical methods

Mineral major element analyses were carried out at the College of Earth Sciences, Guilin University of Technology using a JEOL JXA-8200 electron microprobe. An accelerating voltage of 15 kV, a specimen current of 3.0×10^{-8} A, and a beam size of 1–2 μm were employed. The analytical errors are generally less than 2%. Results are listed in Appendix 1.

Zircons were separated using conventional heavy liquid and magnetic separation techniques. Cathodoluminescence (CL) images were obtained for zircons prior to analysis, using a JEOL JXA-8100 Superprobe at the State Key Laboratory of Isotope Geochemistry, Guangzhou Institute of Geochemistry, Chinese Academy of Sciences (GIG—CAS), in order to characterize internal structures and choose potential target sites for U–Pb dating. LA-ICP-MS zircon U–Pb analyses were conducted on an Agilent 7500 ICP-MS equipped with a 193-nm laser, housed at the State Key Laboratory of Geological Processes and Mineral Resources, Faculty of Earth Sciences, China University of Geosciences (Wuhan). Zircon 91500 was used as the standard (Wiedenbeck et al., 1995) and the standard silicate glass NIST 610 was used to optimize the machine, with a beam diameter of 30 μm. Raw count rates for ^{29}Si, ^{204}Pb, ^{206}Pb, ^{207}Pb, ^{208}Pb, ^{232}Th and ^{238}U were collected, and U, Th, and Pb concentrations were calibrated using ^{29}Si as the internal calibration and NIST 610 as the reference material. ^{207}Pb/^{206}Pb and ^{206}Pb/^{238}U ratios were calculated using the GLITTER program (Jackson et al., 2004). Measured ^{207}Pb/^{206}Pb, ^{206}Pb/^{238}U and ^{208}Pb/^{232}Th ratios in zircon 91500 were averaged over the course of the analytical session and used to calculate correction factors. These correction factors were then applied to each sample to correct for both instrumental mass bias and depth-dependent elemental and isotopic fractionation. Common Pb was corrected by ComPbCorr#3 151 (Andersen, 2002) for those samples with common ^{206}Pb > 1%. Further detailed descriptions of the instrumentation and analytical procedure for the LA-ICP-MS zircon U–Pb technique can be found in Liu et al. (2010). Uncertainties in the ages listed in Appendix 2 are cited as 1σ, and the weighted mean ages are quoted at the 95% confidence level. The age calculations and Concordia plots were made using Isoplot (ver 3.0) (Ludwig, 2003).

Major element oxides were determined by standard X-ray fluorescence (XRF) methods as described by Li et al. (2006). Trace elements were analyzed by inductively coupled plasma mass spectrometry (ICP-MS), using a Perkin-Elmer Sciex ELAN 6000 instrument at GIGCAS. Analytical procedures are similar to those described by Li et al. (2006). Analytical precision for most elements is better than 5%.

Sr and Nd isotopic analyses were performed on a Micromass Isoprobe multi-collector ICP-MS at the GIGCAS, using analytical procedures described by Li et al. (2006). Sr and REE were separated using cation columns, and Nd fractions were further separated with HDEHP-coated Kef columns. Measured ^{87}Sr/^{86}Sr and ^{143}Nd/^{144}Nd ratios were normalized to ^{86}Sr/^{88}Sr = 0.1194 and ^{146}Nd/^{144}Nd = 0.7219, respectively. The reported ^{87}Sr/^{86}Sr and ^{143}Nd/^{144}Nd ratios were adjusted to the NBS SRM 987 standard ^{87}Sr/^{86}Sr = 0.71025 and the Shin Etsu JNdi-1 standard ^{143}Nd/^{144}Nd = 0.512115. Major and trace elements and Sr–Nd isotope results are listed in Table 1.

In situ zircon Hf isotopic analyses were conducted using a Neptune MC-ICP-MS, equipped with a 193-nm laser, at the Institute of Geology and Geophysics, Chinese Academy of Sciences in Beijing, China. During analyses, spot sizes of 32 and 63 μm, with a laser repetition rate of 10 Hz at 100 mJ, were used and raw count rates for ^{172}Yb, ^{173}Yb, ^{175}Lu, ^{176}(Hf + Yb + Lu), ^{177}Hf, ^{178}Hf, ^{179}Hf, ^{180}Hf and ^{182} W were collected. During laser ablation analyses, the isobaric interference of ^{176}Lu on ^{176}Hf is negligible due to the extremely low ^{176}Lu/^{177}Hf in zircon (normally <0.002). However, the interference of ^{176}Yb on ^{176}Hf must be carefully corrected since the contribution of ^{176}Yb to ^{176}Hf could profoundly affect the accuracy of the measured ^{176}Hf/^{177}Hf ratio. In this project, the mean ^{173}Yb/^{171}Yb ratio of the individual spots was used to calculate the fractionation coefficient (β_{Yb}), and then to calculate the contribution of ^{176}Yb to ^{176}Hf. During analysis, an isotopic ratio of ^{176}Yb/^{172}Yb = 0.5887 was applied. The detailed analytical technique is described in Wu et al. (2006). During the analytical period, the

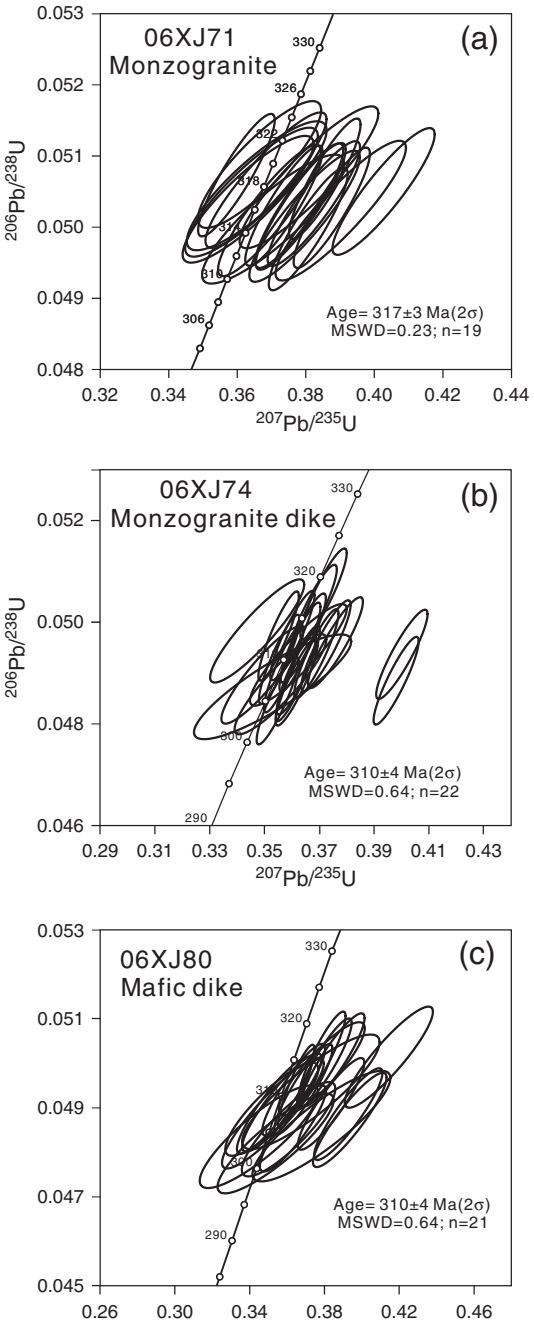

Fig. 4. Concordia diagrams of LA-ICP-MS zircon U–Pb analyses for the monzogranite, monzogranite dike and mafic dike in the Zhongyang pluton (western Tianshan).

$^{176}Hf/^{177}Hf$ and $^{176}Lu/^{177}Hf$ ratios of the standard zircon (91500) were 0.282294 ± 15 ($2\sigma_n$, $n = 20$) and 0.00031, similar to the low peaks of $^{176}Hf/^{177}Hf$ ratios of 0.282284 ± 22 measured by Griffin et al. (2006), also using the laser method. Results are listed in Appendix 3.

4. Results

4.1. Zircon U–Pb geochronology

Zircons in the gabbro dike sample (06XJ80) have crystal lengths of ~100–300 μm and length-to-width ratios from 1:1 to 2:1 and show oscillatory zoning structures in cathodoluminescence (CL) images, which are similar to those from typical gabbros. The analyzed zircon grains have variable Th (26.8-1199 ppm) and U (69.1–902 ppm and 64–9338 ppm, respectively) contents, with Th/U ratios ranging from 0.3 to 1.3, indicating a magmatic origin (Belousova et al., 2002). Twenty one spots were analyzed from 20 zircon grains and give $^{206}Pb/^{238}U$ dates ranging between 303 ± 5 Ma and 316 ± 4 Ma (Appendix 2). They plot on and near Concordia with a weighted mean $^{206}Pb/^{238}U$ age of 310 ± 4 Ma (MSWD = 0.64) (Fig. 4c).

Most zircons in monzogranite (06XJ71) and monzogranite dike (06XJ74) have a size of 60–280 μm a with a length/width ratios of 1:1 to 5:1, and show oscillatory growth zoning. The analyzed zircon grains from samples 06XJ71 and 06XJ74 have variable Th (36.1–368 ppm and 67.6–526 ppm, respectively) and U (60–5310 ppm and 76–6595 ppm, respectively) contents, with Th/U ratios ranging from 0.41 to 0.75 and 0.61 to 0.90, respectively, also indicating a magmatic origin. Nineteen and twenty two U–Pb analyzed spots from samples 06XJ71 and 06XJ74 yielded concordant $^{206}Pb/^{238}U$ dates of 314 ± 3 Ma to 320 ± 4 Ma and 305 ± 4 Ma to 318 ± 4 Ma, with the mean ages of 317 ± 3 Ma (MSWD = 0.23) and 310 ± 4 Ma a (MSWD = 0.64), respectively (Fig. 4a, b; Appendix 2). Therefore, the consistent zircon U–Pb age data for three samples suggest that the Zhongyangchang intrusive rocks were emplaced in the Late Carboniferous (317–310 Ma).

4.2. Major and trace elements

Major and trace element data for the studied mafic dike, granitic intrusion and dike samples are listed in Table 1. These rocks plot in the subalkaline field on the total alkali silica (TAS) diagram. The mafic dikes have low to intermediate contents of SiO_2 (51.61–57.56 wt.%). They are metaluminous with A/CNK ratios [molar $Al_2O_3/(CaO + Na_2O + K_2O)$] of 0.7–0.9, and are medium-K to high-K tholeiitic rocks (Fig. 5). They have a large range of MgO (2.79–5.29 wt.%), Al_2O_3 (13.32–17.20 wt.%), CaO (5.52–8.77 wt.%), Cr (2.86–68.3 ppm), Ni (7.58–32.1 ppm), and relatively high total Fe_2O_3 (10.38–13.93 wt.%) and TiO_2 (0.74–1.60 wt.%) abundances (Fig. 6). The mafic dikes are slightly enriched in light rare earth elements (LREEs) with $(La/Yb)_N$ (where 'N' indicates chondrite-normalized) ratios of 1.2–3.0. They show slightly negative Eu anomalies ($Eu/Eu^* = 0.66–0.94$) in the chondrite-normalized diagrams. The primitive mantle-normalized trace-element distribution patterns of the Zhongyangchang mafic rocks are characterized by the enrichment of large ion lithophile elements (LILEs), such as Rb, Ba, U and K. They are depleted in high field strength elements with strong negative Nb, Ta, P and Ti anomalies (HFSEs) (Fig. 7). The granitoids and granitoid dikes have high SiO_2 contents (65.20–76.58 wt.%) and are metaluminous to

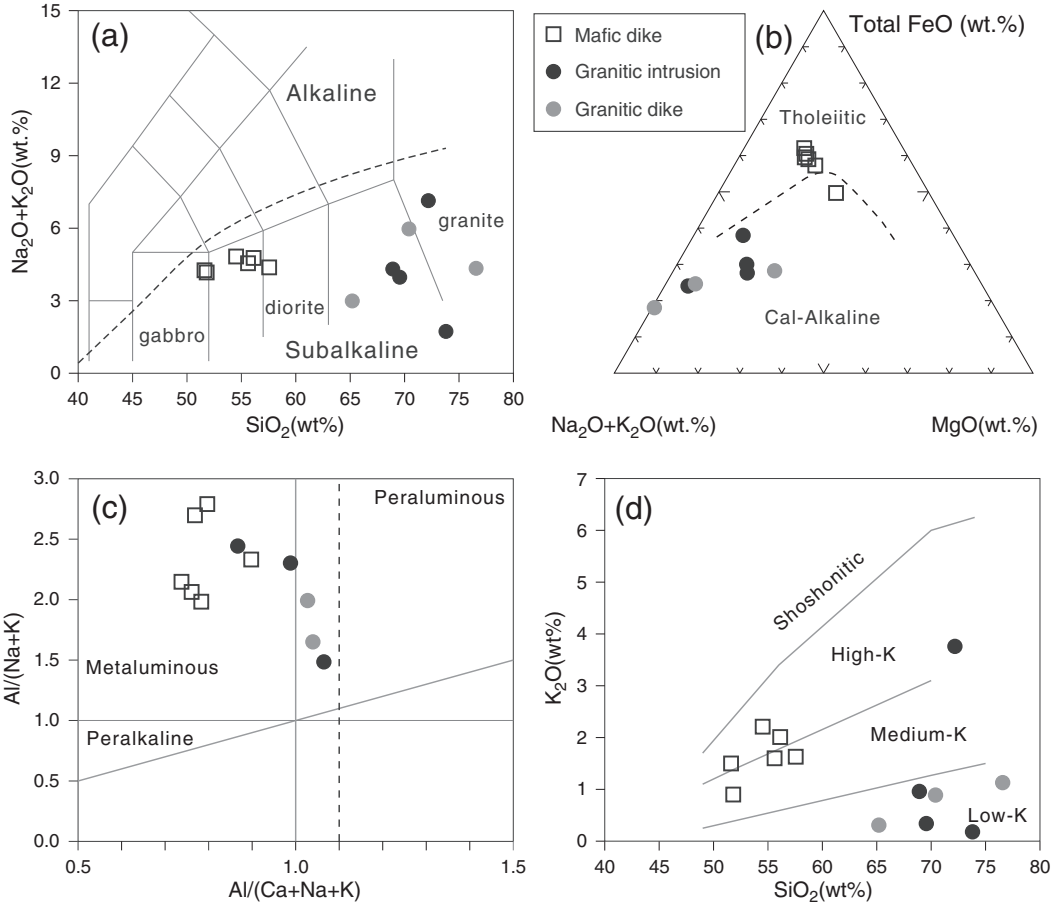

Fig. 5. (a) TAS diagram (Middlemost, 1994); the dashed line separating alkaline series from subalkaline series is from Irvine and Baragar (1971). (b) AFM plot (Irvine and Baragar, 1971). (c) A/NK [molar ratio $Al_2O_3/(Na_2O + K_2O)$] vs. A/CNK [molar ratio $Al_2O_3/(CaO + Na_2O + K_2O)$]. (d) SiO_2–K_2O plot (Peccerillo and Taylor, 1976).

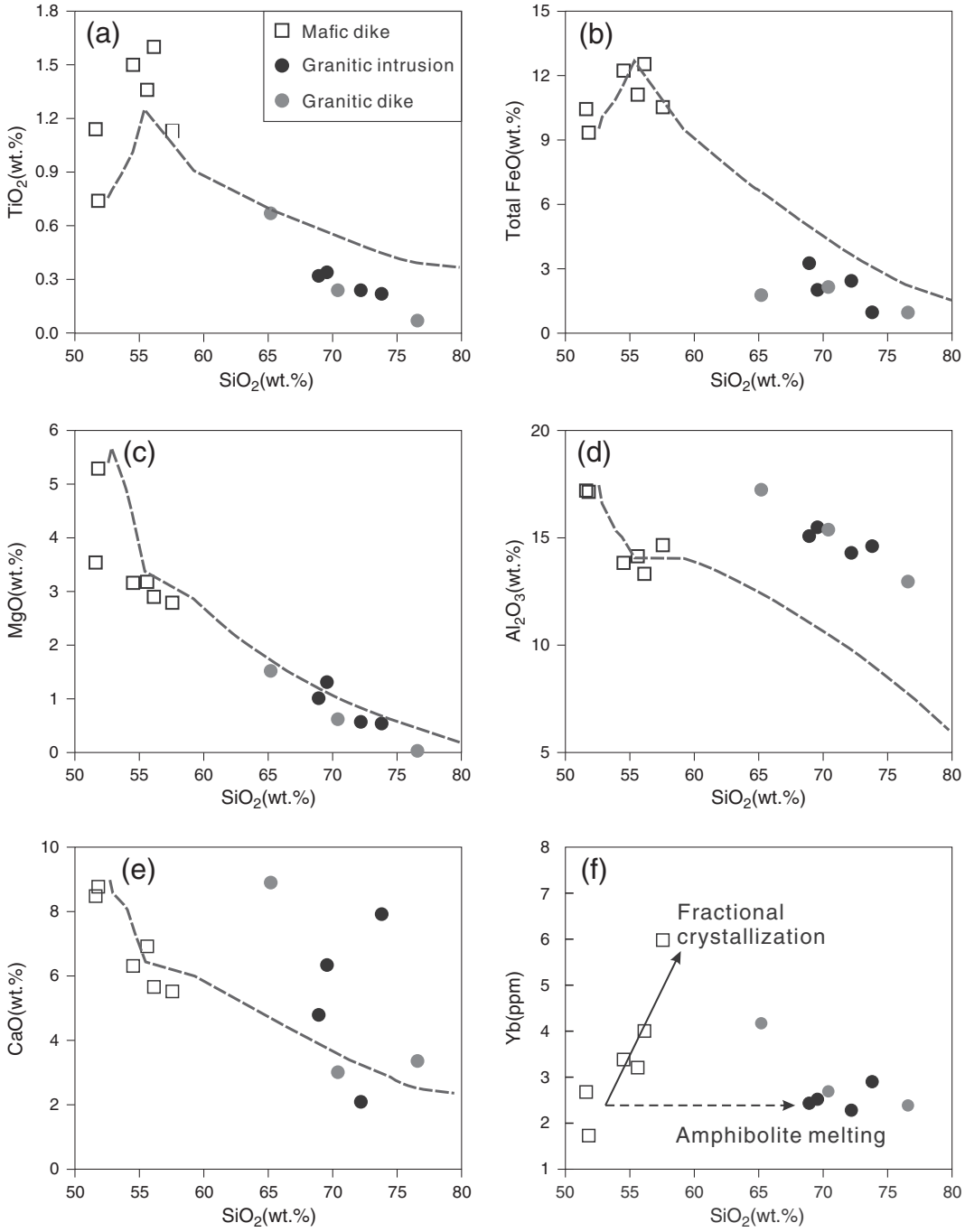

Fig. 6. Various element plots for Zhongyangchang rocks from western Tianshan. (a) TiO_2, (b) Total FeO, (c) MgO, (d) Al_2O_3, (e) CaO, and (f) Yb vs. SiO_2 diagrams. The dotted lines represent results of fractional crystallization modeling using MELTS (Ghiorso and Sack, 1995) plotted on a–e. Model assuming a starting composition of 06XJ80 at pressures of 3 kbar, fO_2 = NNO + 1 and H_2O = 3.0 wt.%. Fractional crystallization and amphibolite melting paths using the model results of Brophy (2008), that are independent of the type of melting involved (equilibrium, fractional, accumulated fractional).

weakly peraluminous with A/CNK of 0.8–1.1 (Fig. 5). With the exception of one sample, they belong to the low-K suite, with Na_2O/K_2O ratios greater than l. They have relatively low MgO, TiO_2, total Fe_2O_3, Cr and Ni concentrations. They are enriched in LREEs relative to heavy REEs with $(La/Yb)_N$ ratios of 1.9–6.6. They have weak to strong negative Eu anomalies, with Eu/Eu* values of 0.1–1.0. On primitive mantle-normalized trace element diagrams, they are enriched in LILEs, such as Rb, Ba, Th and U and depleted in HFSEs with negative Nb, Ta, P and Ti anomalies (Fig. 7).

4.3. Sr–Nd–Hf isotopic compositions

The whole rock initial $^{87}Sr/^{86}Sr$ ratios, $\varepsilon_{Nd}(t)$ and zircon $\varepsilon_{Hf}(t)$ values have been calculated at 317–310 Ma on the basis of the zircon U–Pb ages for these rocks. The mafic dikes have low $^{87}Rb/^{86}Sr$ ratios of 0.20–0.48, and have a low and narrow range of initial $^{87}Sr/^{86}Sr$ ratios from 0.7048 to 0.7053, with relatively high $\varepsilon_{Nd}(t)$ values from +2.9 to +3.8. The granitoids and granitoid dikes also have low $^{87}Rb/^{86}Sr$ ratios of 0.05–0.58, with the exception of one sample of monzogranite that

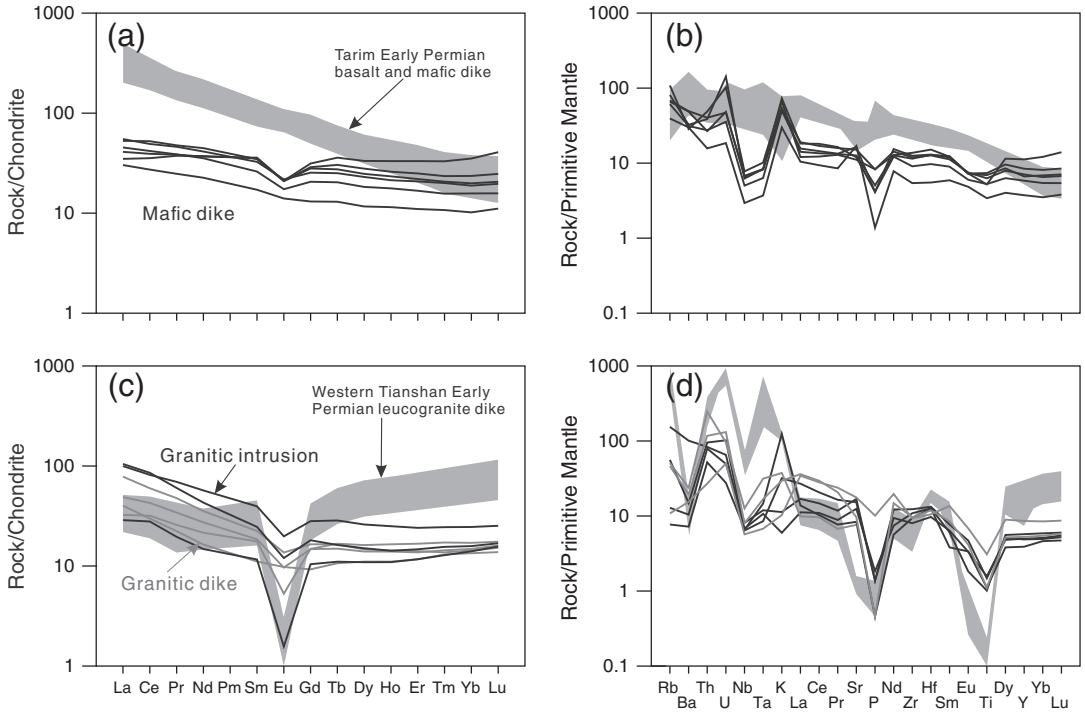

Fig. 7. Chondrite-normalized rare earth element patterns and primitive mantle normalized trace element diagrams for mafic dikes (a and b), and granitoids (c and d) of the Zhongyangchang pluton. Tarim Early Permian basalt and mafic dike (Wei et al., 2014; Zhou et al., 2009) and Western Tianshan Early Permian leucogranite dike (Gao et al., 2011) are shown for comparison. The chondrite and primitive mantle values are from Sun and McDonough (1989).

shows high $^{87}Rb/^{86}Sr$ ratios of 1.61. All of these rocks have Sr and Nd isotopic compositions lying within a narrow range of initial $^{87}Sr/^{86}Sr$ and $\varepsilon_{Nd}(t)$ values, from 0.7045 to 0.7056, and from +0.2 to +2.8, respectively. The felsic rocks have slightly lower $\varepsilon_{Nd}(t)$ values than the mafic rocks, although they have identical initial $^{87}Sr/^{86}Sr$ values (Fig. 8).

Two zircons from mafic dike sample of 06XJ80 were analyzed for Hf isotopic compositions, giving identical initial $^{176}Hf/^{177}Hf$ ratios from 0.292922 to 0.282960 and depleted $\varepsilon_{Hf}(t)$ values from +12.2 to +13.6. The monzogranite and monzogranite dike (06XJ71 and 06XJ74) have variable zircon Hf isotopic compositions, with initial $^{176}Hf/^{177}Hf$ ratios of 0.282762–0.283011, $\varepsilon_{Hf}(t)$ values of +6.6 to +15.3 and T_{DM} values of 0.36–0.77 Ga (Fig. 8, Appendix 3).

5. Discussion

5.1. Petrogenetic characteristics of the mafic dike

The mafic dikes of the Zhongyangchang pluton show low SiO_2 (51.81–57.56 wt.%), relative to continental crust (Rudnick and Gao, 2003) or crust-derived melts (Patiño Douce and Beard, 1995), indicating that they were derived from a mantle source. However, the mafic dikes have relatively low MgO (less than 5.29 wt.%), Cr (2.86–68.3 ppm) and Ni (7.28–32.1 ppm) contents relative to the melts derived from partial melting of peridotites, indicating that their parental magmas experienced crystal fractionation of olivine, pyroxene, amphibole and plagioclase. The strong depletion of Nb and Ta for the Zhongyangchang mafic dikes may suggest involvement of a continental crust component in the magmas (Fig. 7b), because the continental crust is typically depleted in these elements (Rudnick, 1995). Therefore, fractional crystallization and crustal contamination need to be assessed for the mafic dikes prior to further petrogenetic analysis.

The $\varepsilon_{Nd}(t)$ values of the Zhongyangchang dikes correlate positively with MgO, indicating that crustal contamination processes may have acted on their parental magmas (Fig. 9a). Country rocks in the studied area include Carboniferous granitoids. They are characterized by positive $\varepsilon_{Nd}(t)$ values in this study, however, which indicates that they do not represent a suitable contaminant (Fig. 8a). In addition, $\varepsilon_{Nd}(t)$ values of the mafic dikes are negatively correlated with variable Nb/La ratios (Fig. 9b), which is inconsistent with crustal contamination processes given that continental crust is typically characterized by low $\varepsilon_{Nd}(t)$ and low Nb/La ratio relative to that of the mantle (Rudnick, 1995). The positive correlation between Nb/La and SiO_2 and the negative correlation between Nb/La and MgO are also inconsistent with crustal contamination processes (Fig. 9c–d). Thus, the Nb–Ta deficits in the Zhongyangchang mafic dikes were inherited from their source, rather than from crustal contamination.

Ratios involving HFSE and REE are commonly used to assess the mantle sources of mafic rocks. Amphibole fractionation, however, can change HFSE and REE ratios because Nb, Ta, Ti and MREE are all compatible in amphibole (Klein et al., 1997; Tiepolo and Tribuzio, 2008). In addition, primary amphibole phenocrysts are present in the Zhongyangchang mafic dikes (Fig. 2d). A useful approach to estimate the effect of amphibole fractionation employs a plot of Dy/Dy* vs Dy/Yb (Fig. 10a) (Davidson et al., 2013). With the exception of two samples with the highest SiO_2 content (06XJ68 and 76), the mafic dikes show clear trends parallel to the amphibole fractionation curve, indicating that amphibole fractionation has occurred. At the same time, however, these low SiO_2 mafic dike samples all fall within the MORB array and therefore they are used to investigate the mantle source.

The Nb–Ta depletions, relative to the LREE, in the Zhongyangchang mafic dikes may reflect the contribution of fluids and/or melts derived from the subducting slab. The log–log Nb/Y–Zr/Y plot has proven to be a robust discriminant between basalts derived from DMM source regions and from mantle plumes (oceanic island and plateau basalts) and Zr/Y and Nb/Y ratios display only small variations with low-pressure crystal fractionation and partial melting processes (Fitton et al., 1997). The plot defines a mantle array that is also insensitive to the effects of hydrous fluid metasomatism (Fig. 10b). All of the mafic dikes fall along the mantle array, suggesting that slab-derived fluids, and not melts, contributed to the mantle sources. The analogous Zr/Yb vs Nb/

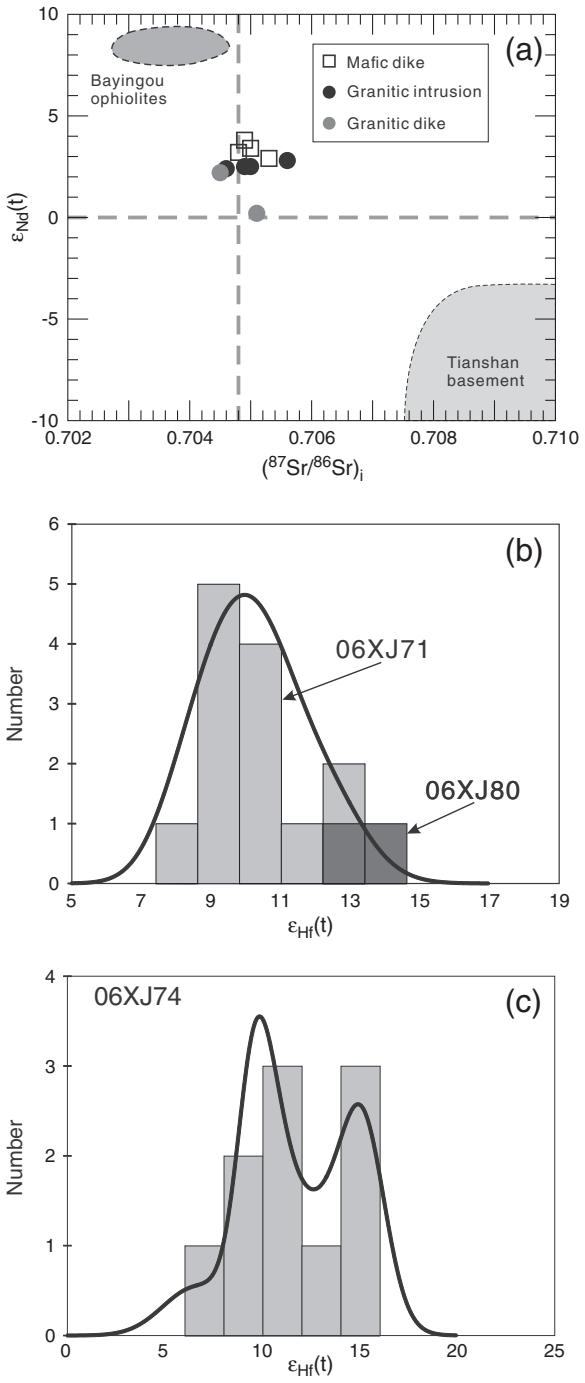

Fig. 8. (a) $\varepsilon_{Nd}(t)$ vs. $(^{87}Sr/^{86}Sr)_i$, probability diagrams of $\varepsilon_{Hf}(t)$ values of zircons in (b) mafic rocks (06XJ80) and granitic porphyry (06XJ71), and (c) granitic dike.

Yb plot (Fig. 10c) indicates that the Zhongyangchang mafic dikes were derived entirely from depleted MORB-source mantle. The depleted Nd–Hf isotopic compositions also argue against a scenario where isotopically enriched slab-derived sediments were introduced into mantle sources through partial melting or bulk addition. The Zhongyangchang mafic dikes are q–hy-normative, indicating a pressure of magma segregation of 15–20 kbar, based on the experimental results for the partial melting of anhydrous mantle peridotites (Hirose and Kushiro, 1993; Takahashi and Kushiro, 1983). Flat Chondrite-normalized HREE patterns also suggest that melting took place within the spinel stability field. This relatively shallow depth of melt extraction is further supported by REE modeling. The Gd/Yb ratio can effectively discriminate the fingerprint of spinel from garnet in the mantle source. Ytterbium is compatible in garnet with a higher phase/melt partition coefficient for Yb than Gd, whereas spinel has similar phase/melt partition coefficients for both of these elements. The Zhongyangchang mafic dikes have low Dy/Yb and Gd/Yb ratios (Fig. 10d), which plot on the melting curve of spinel peridotite with no garnet in the source, suggesting that the magmas were generated at a relatively shallow depth, mostly within the spinel stability field with variable degrees (5–10%) of batch melting of an upper mantle source.

5.2. Petrogenesis of the granitoids

The granitoid plutonic and dike samples have identical geochemical and Sr–Nd and zircon Hf isotopic compositions (Fig. 8), indicating a common source or petrogenetic process. They have relatively low MgO, Cr and Ni contents at high silica concentrations. These calc-alkaline and metaluminous geochemical features are considered to be the products of mixing between mantle- and crust-derived magmas (Barbarin, 2005; Tang et al., 2012b; Yang et al., 2007a), fractional crystallization of mantle derived basaltic magma (Barth et al., 1995), or partial melting of juvenile sub-alkaline metabasaltic rocks (Patiño Douce and Beard, 1995; Rapp, 1995; Rapp et al., 1999).

The physical and geochemical characteristics of the Zhongyangchang granitoids are inconsistent with mixing of mantle- and crust-derived melts. No mafic microgranular mafic enclaves (MME) have been found in the pluton and plagioclases from the granitoids all show simple normal zoning (Fig. 4) with no evidence for magma mixing. Furthermore, these granitoids have a narrow range of Nd–Hf isotopic compositions (Fig. 8), which is also inconsistent with magma mixing that generally results in a wide range of isotopic compositions. Based on several lines of evidence below, fractional crystallization of basaltic magma can also be excluded, although the mafic dikes and granitoids have similar Sr–Nd–Hf isotopic compositions (Fig. 8). We attempted to model the fractionation history of the basaltic rocks using MELTS (Ghiorso and Sack, 1995; Smith and Asimow, 2005). We use 3 kbar pressure, water content of 3 wt.% and fO_2 = NNO + 1 and a starting composition of basaltic rocks (06XJ80) to test the fractionation hypothesis (Fig. 6a–e). Modeling results show that fractionation did not generate major element compositions similar to the granitoids. In addition, Brophy (2008) suggested that a crystal fractionation origin for felsic magmas will generate positive trends between SiO_2 and REE concentrations, whereas dehydration melting of amphibolite crust leads to negative SiO_2–REE correlations. The granitoids have lower REE levels than the mafic dikes (Fig. 6f), which is inconsistent with an origin via differentiation of the basaltic magma. Furthermore, no rocks compositionally intermediate between the mafic dikes and the granitoids have been identified in the area.

The Zhongyangchang granitoids have low initial $^{87}Sr/^{86}Sr$ ratios (0.7045–0.7056), positive whole rock $\varepsilon_{Nd}(t)$ (+0.2 to +2.8) and zircon $\varepsilon_{Hf}(t)$ (+6.6 to +15.3) values with young Nd (0.85–1.1 Ga) and Hf (0.36–0.77 Ga) model ages, indicating that they may have been derived from a crustal source formed by underplating of depleted mantle-derived mafic magmas during the Late Carboniferous. The Sr–Nd–Hf isotopic data for the mafic dikes are similar to those of the granitoids, which suggests that the hypothesized underplated basaltic magmas correspond to the parental magmas of the Zhongyangchang mafic dikes. Experimental results can provide insight into the melt compositions produced from different sources and P–T conditions of melt generation (Fig. 11a–b). The Zhongyangchang granitoids have intermediate Na_2O and low K_2O contents at high silica contents, identical to the compositions of melts produced by partial melting of amphibolites (Beard and Lofgren, 1991). In order to evaluate this process we use REE data to model batch partial melting (Fig. 11c). Mafic dike of 06XJ80 was selected as a proxy of juvenile lower crust beneath the study area. We assume that the partial melting took place under an amphibolite-facies condition and the initial mineralogical assemblages were Amph

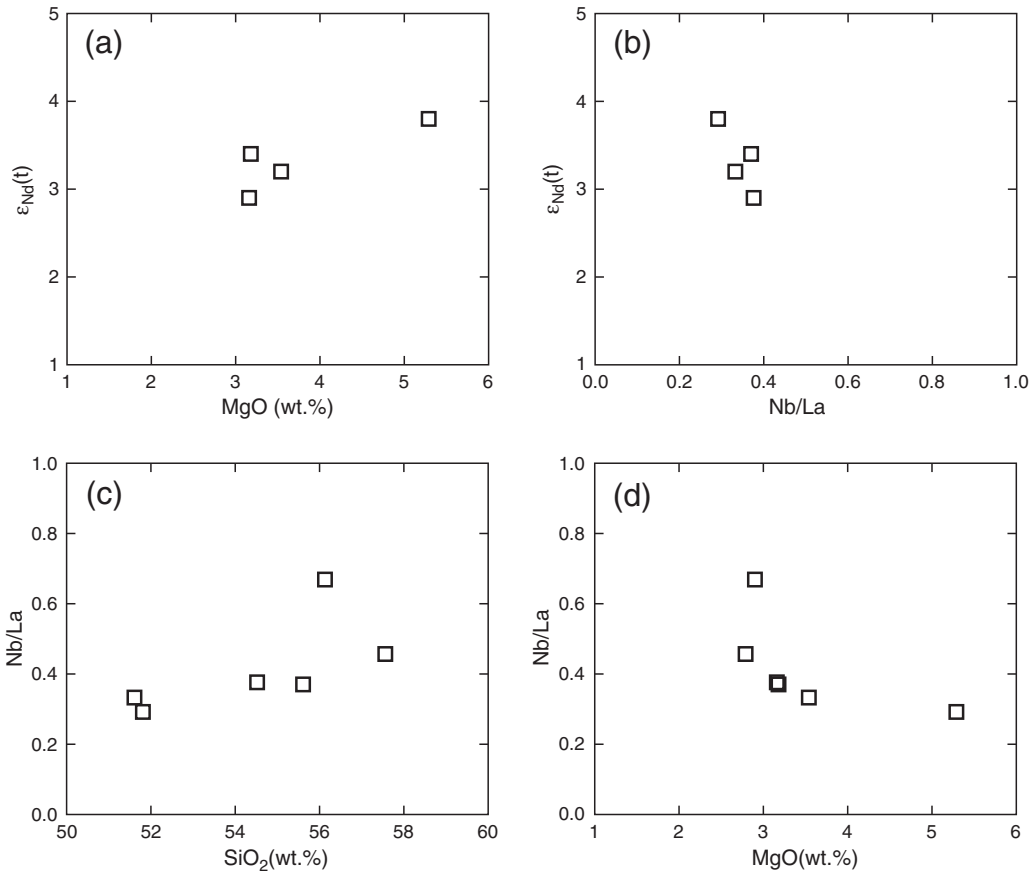

Fig. 9. Plots of $\varepsilon_{Nd}(t)$ vs. MgO and Nb/La (a and b), and Nb/La vs. SiO_2 and MgO (c and d) for mafic dikes of the Zhongyangchang pluton from the western Tianshan.

(amphibole):Plag (plagioclase):Cpx (clinopyroxene) = 50:25:25. The chondrite-normalized REE pattern for the Zhongyangchang granitoids is reproduced by 15% batch melting (Fig. 11c).

In summary, the mafic dikes with low initial $^{87}Sr/^{86}Sr$ ratios and positive $\varepsilon_{Nd}(t)$ and $\varepsilon_{Hf}(t)$ values were formed by partial melting of depleted lithospheric mantle source, fluxed by fluids derived from the downgoing slab. The granitoids in the Zhongyangchang pluton also have low initial $^{87}Sr/^{86}Sr$ ratios and positive $\varepsilon_{Nd}(t)$ and $\varepsilon_{Hf}(t)$ values with young Nd and Hf model age, indicating a juvenile crustal origin. Collectively, the geochronological, chemical and isotopic evidence require that the granitoids were generated by partial melting of juvenile basaltic lower crust as a result of magma underplating.

5.3. Tectonic implications

Mafic dike–granitoid associations are common in extensional tectonic regimes that are usually interpreted as post-collisional or intraplate extensional settings (Said and Kerrich, 2010; Xu et al., 2008; Yang et al., 2007b). Most recently, a mantle plume model has been invoked to account for the Tianshan and Junggar mafic dikes, because the mafic dikes purportedly formed in the Early Permian (290–260 Ma), coeval with the Tarim large igneous province (Zhang and Zou, 2013). However, numerous zircon U–Pb and whole rock or amphibole $^{40}Ar/^{39}Ar$ dating results indicate that mafic dikes in the west Junggar and Tianshan regions formed during the Late Carboniferous (~320–305 Ma) (Feng et al., 2012; Tang et al., 2012b; Yin et al., 2010, 2013) and are unequivocally older than the Early Permian (275 Ma) Tarim large igneous province (Wei et al., 2014). In addition, the geochemical characteristics of the Zhongyangchang mafic dikes are distinct from those of the Tarim Early Permian basalts and mafic dikes (Fig. 7a–b). Zhongyangchang mafic dikes have low LREE contents with flat chondrite-normalized patterns, and show strongly negative Nb, Ta, Ti and P anomalies. In contrast, Tarim Early Permian basalts and mafic dikes display more fractionated REE patterns, without pronounced peaks at Nb, Ta and Ti. Thus, these Late Carboniferous mafic dikes are unlikely to have originated from the Tarim mantle plume.

The Late Carboniferous Zhongyangchang mafic dikes and granitoids are also unlikely to have formed in a post-collisional setting. There is growing evidence for the Junggar oceanic crust subducted south beneath the western Tianshan during the Late Carboniferous, forming a northwest Tianshan Carboniferous arc along the northern margin of the Yili Block (An et al., 2013; Long et al., 2011; Zhu et al., 2009). Their geochemical characteristics are also inconsistent with an origin during post-collisional events. The mafic dikes are enriched in LILE and depleted in HFSE, with strongly negative Nb–Ta anomalies, indicating an arc origin. All mafic dikes fall into the area of arc-basalts on a Hf/3–Th–Nb/16 tectonic discriminant diagram (Fig. 12a). The Zhongyangchang Late Carboniferous granitoids also all plot in the volcanic arc field on the Yb–Ta tectonic discrimination diagram. They are distinct from Early Permian (285 Ma) strongly peraluminous leucogranite dikes from the South Tianshan Orogen that all fall into the within plate granite field, which formed as a result of exhumation of over-thickened crusts in a post-collisional setting (Figs. 7c–d, 12b) (Gao et al., 2011). In addition, the other Late Carboniferous basaltic rocks from the western Tianshan all show typical island arc type geochemical characteristics, suggesting that their origin was related to oceanic subduction (Tang et al., 2012a). Furthermore, Carboniferous ophiolites have recently been identified in the area, e.g., the 344 ± 3 Ma Bayingou ophiolite in the western Tianshan (Xu et al., 2006). This ophiolite is only slightly older than the Zhongyangchang intrusive rocks. Therefore, diverse

types of evidence overwhelmingly indicate that the Late Carboniferous Zhongyangchang mafic dike–granitoids association was not related to a post-collisional setting, but rather formed at an arc setting related to oceanic subduction.

The Late Paleozoic magmatism in the Tianshan Orogen can be roughly divided into three main episodes encompassing the Late Devonian to Early Carboniferous, Late Carboniferous and Early Permian, as suggested by a histogram of zircon U–Pb age data (Fig. 13). The Late Devonian to Early Carboniferous magmatic rocks consist mainly of calc-alkaline granitoids, and volcanic rocks including basalt, trachyte, trachyandesite, andesite and rhyolite (An et al., 2013; Long et al., 2011; Tang et al., 2010; Zhu et al., 2009). All of these rocks show typical arc-like geochemical characteristics (e.g., enrichment of large ion lithophile elements (LILE) and strong negative anomalies of Ta, Nb, P and Ti). A significant Late Carboniferous magmatic "flare-up" event occurred in the Tianshan orogen. The resulting magmatic rocks ranged from basaltic to rhyolitic in composition similar to the Late Devonian to Early Carboniferous magmatic rocks. At the same time, many Late Carboniferous mafic rocks were emplaced in the western Tianshan, e.g., the Luotuogou gabbroic pluton (312 Ma, Tang et al., 2012a) and Haladala gabbroic pluton (306 Ma, Zhu et al., 2010). Recent studies suggested that these Late Carboniferous mafic rocks were derived from a depleted mantle source containing an asthenospheric component. It is noteworthy that a magmatic gap or quiescent period existed between the Late Carboniferous and Early Carboniferous (Fig. 13). The Early Permian magmatic rocks consist mainly of A-type granites (Tang et al., 2010). Early Permian strongly peraluminous leucogranite dike, crosscutting the high pressure-low temperature Tianshan metamorphic belt, also indicates the Tianshan Orogen entered into a post-collision setting during that time (Gao et al., 2011).

Taking into account all available data from Late Paleozoic magmatic rocks in the western Tianshan region, we prefer a slab roll-back model during the Late Carboniferous (Fig. 13) because it can readily account for the Late Carboniferous magmatic "flare-up" and the presence of subordinate mafic rocks, which required an asthenospheric component (Fig. 14). It is most likely that normal subduction produced the Late Devonian to Early Carboniferous magmatic rocks, but was followed by a period of "flat-subduction" that resulted in an interval of magmatic quiescence. Finally, the oceanic slab was likely to have undergone roll-back to normal, steeper, angles of subduction during the Late Carboniferous. A descending slab migrating backwards in the asthenospheric mantle (roll-back) would cause asthenosphere upwelling. On the one hand, this process provides heat to melt overlying metasomatized lithospheric mantle and on the other hand, it provides an upwelling asthenospheric mantle component for mafic magmas. Sustained mafic magma underplating eventually leads to partial melting of juvenile basaltic lower crust, producing felsic rocks.

6. Conclusions

The Zhongyangchang intrusive rocks in the western Tianshan are mainly composed of mafic dikes, plutonic granodiorite and monzogranite, and minor granitic dikes. New zircon U–Pb ages indicate that the Zhongyangchang intrusive rocks were all emplaced in the Late

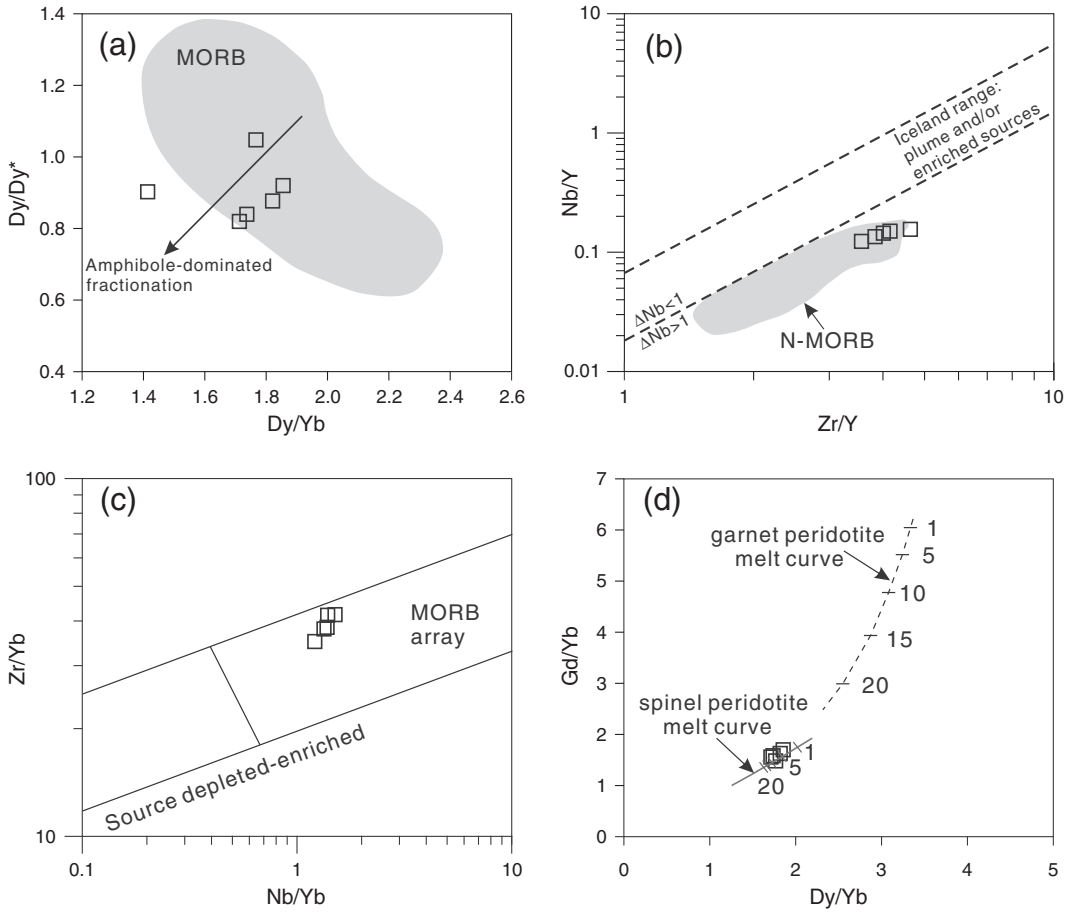

Fig. 10. (a) Dy/Dy* vs Dy/Yb after Davidson et al. (2013). (b) Nb/Y vs Zr/Y after Fitton et al. (1997) showing separation of MORB-source and enriched, plume*like mantle sources. (c) Zr/Yb vs Nb/Yb after Pearce and Peate (1995). (d) Non-modal batch melting model for Gd/Yb vs Dy/Yb, using the equation of Shaw (1970). Ticks along the curves indicate the degree of melting in percent. Melting modes are from Thirlwall et al. (1994). Initial abundances of DMM are from Workman and Hart (2005). Partition coefficients from Kelemen et al. (1993), Tiepolo et al. (2003) and Foley (2008).

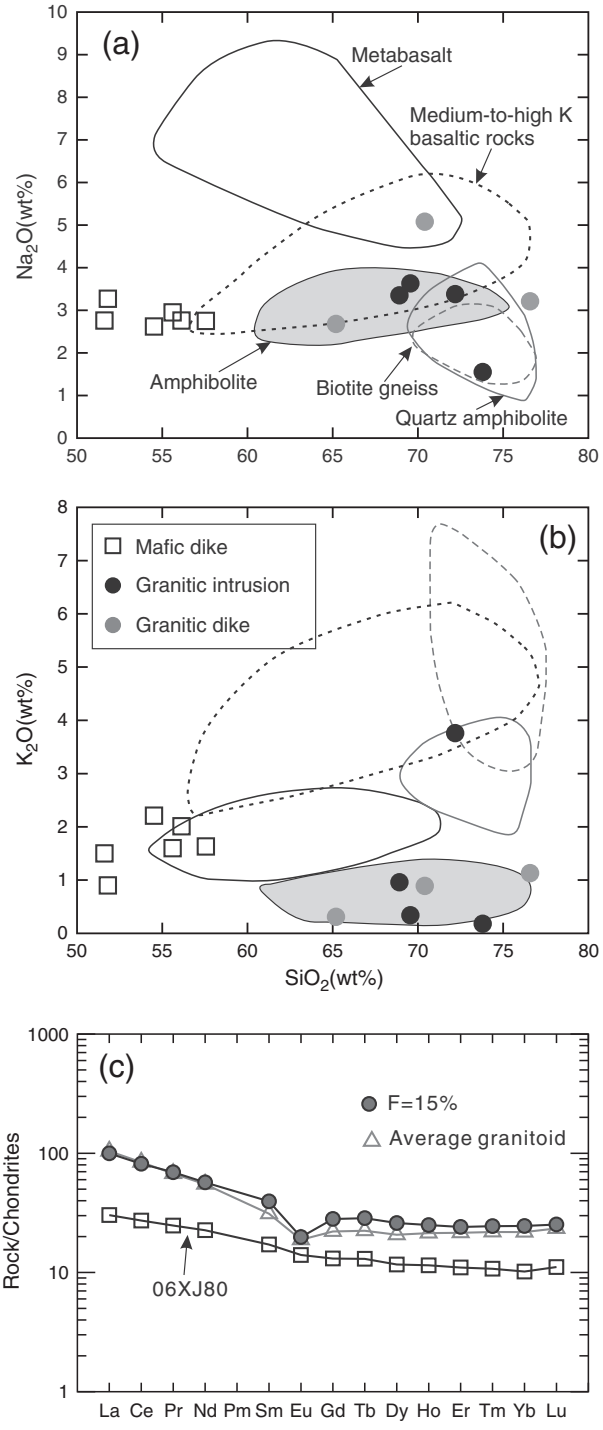

Fig. 11. SiO_2 vs. Na_2O and K_2O for granitoids of the Zhongyangchang pluton compared to experimental melts (a–b). Experimental melts are from Beard and Lofgren (1991) (amphibolites; 1, 3, 6, 9 kb; 800–1000 °C), Rapp and Watson (1995) (metabasalt; 8–32 kb; 1000–1125 °C), Patiño Douce and Beard (1995) (quartz amphibolites; 3–15 kb; 850–930 °C); Patiño Douce and Beard (1995) (biotite gneiss; 3–15 kb; 850–930 °C) and Sisson et al. (2005) (medium to high K basaltic rocks; 700 Mpa; 825–975 °C). (c) (b) REE modeling patterns for Zhongyangchang granitoids showing melt curves by batch partial melting. The REE partition coefficients are from McKenzie and O'Nions (1991).

Carboniferous (317–310 Ma), establishing that the mafic and felsic magmas were coeval. The petrographic and geochemical data, Sr–Nd isotopic and zircon Hf isotopic compositions indicate that the parental magma of the Late Carboniferous Zhongyangchang mafic rocks was derived from a depleted lithospheric mantle source, fluxed by fluids derived from the down-going slab. The granitoids

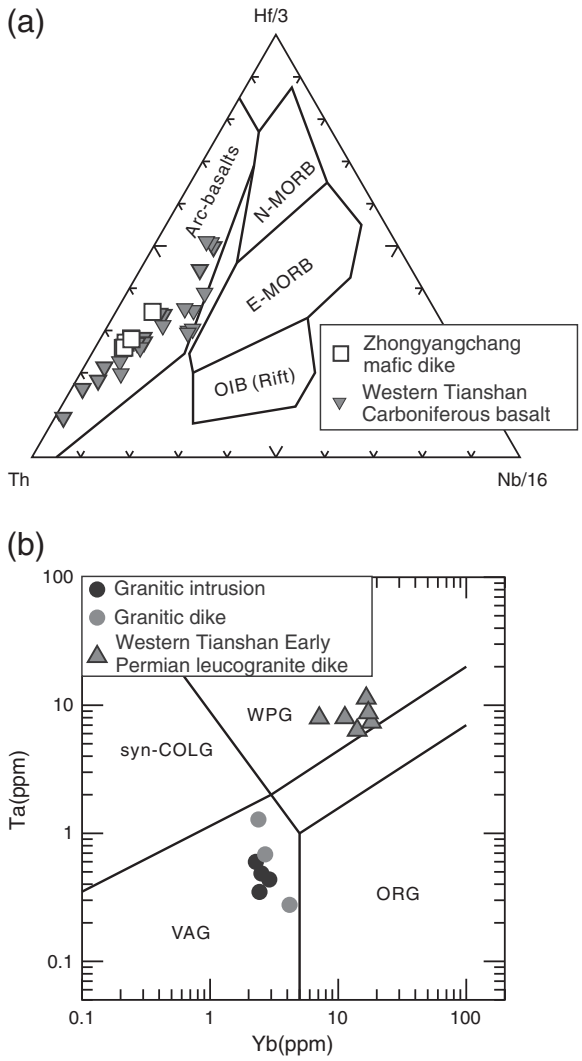

Fig. 12. (a) The Zhongyangchang mafic dikes on the Th–Nb/16–Hf/3 discrimination diagram of Wood (1980). Western Tianshan Carboniferous basalts are shown for comparison (An et al., 2013; Long et al., 2011; Zhu et al., 2009). (b) Tectonic discrimination plot for granites (Pearce et al., 1984) and western Tianshan Early Permian leucogranite dikes are shown for comparison (Gao et al., 2011).

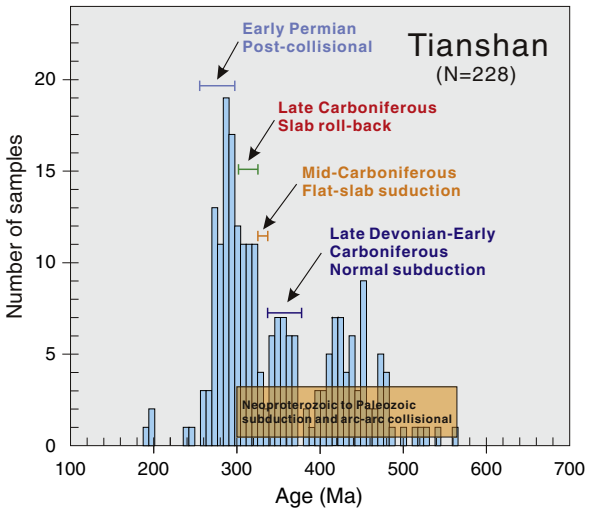

Fig. 13. Histogram of zircon U–Pb ages for granitoids of the Tianshan orogen. Modified after Seltmann et al. (2011) and Xiao et al. (2013).

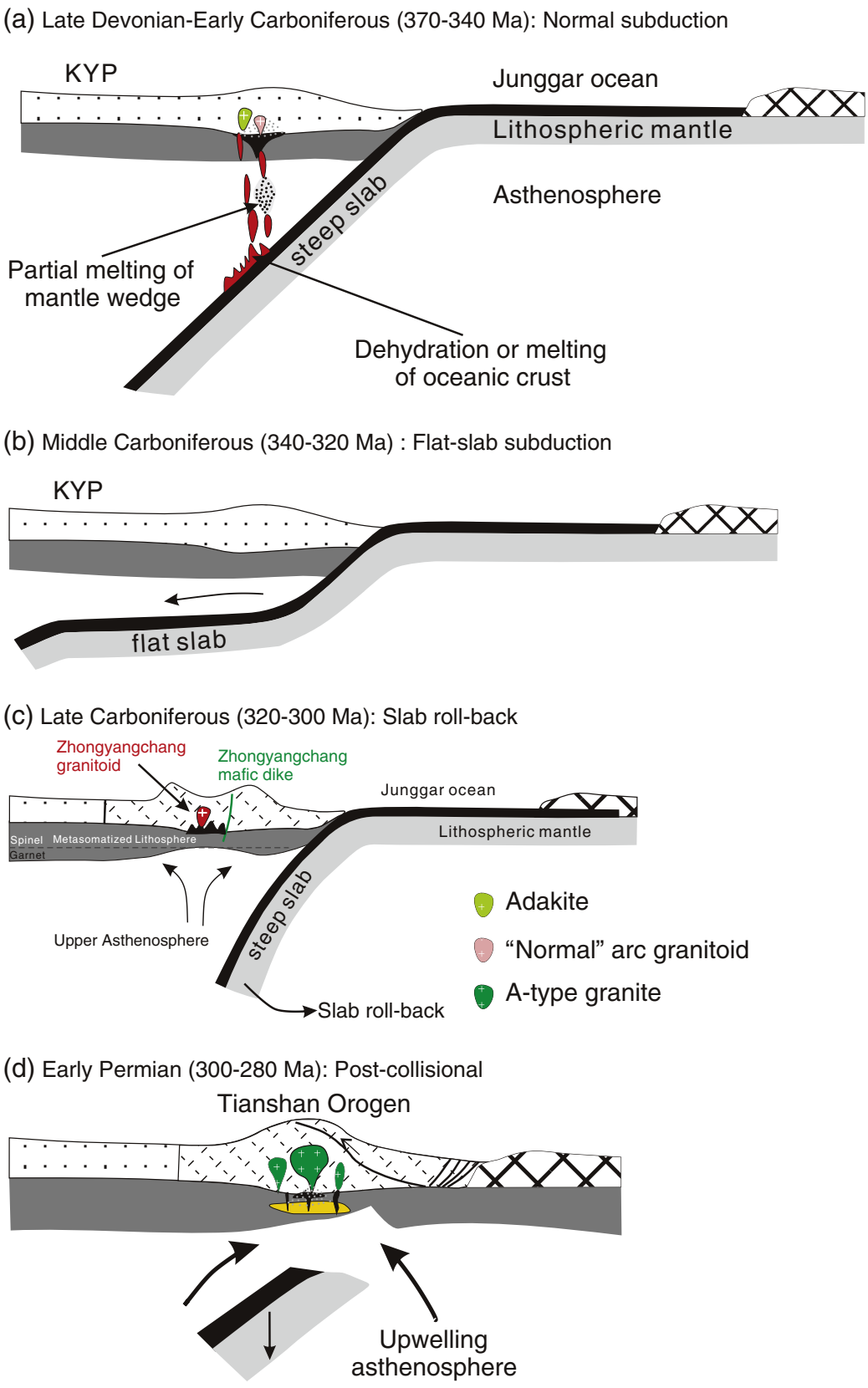

Fig. 14. Schematic diagrams for the Late Paleozoic tectonic evolution of the western Tianshan. Modified after Tang et al. (2010, 2012a).

in the Zhongyangchang pluton also have low initial $^{87}Sr/^{86}Sr$ ratios and positive $\varepsilon_{Nd}(t)$ and $\varepsilon_{Hf}(t)$ values similar to those of mafic rocks, with young Nd and Hf model ages. The granitoids were generated by partial melting of juvenile basaltic lower crust as a result of magma underplating. The Late Carboniferous mafic dike–granitoid association was not related to a post-collisional setting, but rather

formed at an arc setting related to oceanic subduction. The most likely tectonic model accounting for the genesis of these rocks involves an extensional environment in the western Tianshan during the Late Carboniferous as a tectonic response to the roll-back of subducted Junggar oceanic lithosphere, which could accounts for the "flare-up" of Late Carboniferous magmatism.

Supplementary data to this article can be found online at http://dx.doi.org/10.1016/j.lithos.2014.04.010.

Acknowledgments

This study was supported by funding from the Strategic Priority Research Program (B) of the Chinese Academy of Sciences (grant no. XDB03010600), the Major State Basic Research Program (973 Program) of the People's Republic of China (no. 2011CB808906), the National Natural Science Foundation of China (grant nos. 41025006 and 41202041) and the Outstanding Young Researchers Foundation of the State Key Laboratory of Isotope Geochemistry (grant no. SKLIG-RC-13-01). The senior author thanks the grant from the National Science Council Taiwan, which supported his one-year academic visit at the NTU. This is contribution no. 1896 from GIG—CAS.

References

Allen, M.B., Windley, B.F., Zhang, C., 1993. Palaeozoic collisional tectonics and magmatism of the Chinese Tien Shan, central Asia. Tectonophysics 220, 89–115.
An, F., Zhu, Y., Wei, S., Lai, S., 2013. An Early Devonian to Early Carboniferous volcanic arc in North Tianshan, NW China: geochronological and geochemical evidence from volcanic rocks. Journal of Asian Earth Sciences 78, 100–113.
Andersen, T., 2002. Correction of common lead in U–Pb analyses that do not report ^{204}Pb. Chemical Geology 192, 59–79.
Barbarin, B., 2005. Mafic magmatic enclaves and mafic rocks associated with some granitoids of the central Sierra Nevada batholith, California: nature, origin, and relations with the hosts. Lithos 80, 155–177.
Barth, A.P., Wooden, J.L., Tosdal, R.M., Morrison, J., 1995. Crustal contamination in the petrogenesis of a calc-alkalic rock series: Josephine Mountain intrusion, California. Geological Society of America Bulletin 107, 201–212.
Beard, J.S., Lofgren, G.E., 1991. Dehydration melting and water-saturated melting of basaltic and andesitic greenstones and amphibolites at 1, 3, and 6, 9 kb. Journal of Petrology 32, 365–401.
Belousova, E., Griffin, W., O'Reilly, S.Y., Fisher, N., 2002. Igneous zircon: trace element composition as an indicator of source rock type. Contributions to Mineralogy and Petrology 143, 602–622.
Brophy, J., 2008. A study of rare earth element (REE)-SiO_2 variations in felsic liquids generated by basalt fractionation and amphibolite melting: a potential test for discriminating between the two different processes. Contributions to Mineralogy and Petrology 156, 337–357.
Carroll, A.R., Graham, S.A., Hendrix, M.S., Ying, D., Zhou, D., 1995. Late Paleozoic tectonic amalgamation of northwestern China; sedimentary record of the northern Tarim, northwestern Turpan, and southern Junggar basins. Geological Society of America Bulletin 107, 571–594.
Charvet, J., Shu, L., Laurent-Charvet, S., Wang, B., Faure, M., Cluzel, D., Chen, Y., De Jong, K., 2011. Palaeozoic tectonic evolution of the Tianshan belt, NW China. Science China Earth Sciences 54, 166–184.
Davidson, J., Turner, S., Plank, T., 2013. Dy/Dy*: variations arising from mantle sources and petrogenetic processes. Journal of Petrology 54, 525–537.
Eby, G.N., 1992. Chemical subdivision of the A-type granitoids: petrogenetic and tectonic implications. Geology 20, 641–644.
Feng, Q.W., Li, J.Y., Liu, J.F., Song, B., Wang, Y.B., Chen, W., Zhang, Y., 2012. Ages and geological significance of the dark dykes emplaced in the Karamay pluton and adjacent area, in western Junggar, Xinjiang, NW China: evidence form LA-ICP-MS zircon chronology and Ar–Ar amphibole chronology. Acta Petrologica Sinica 28, 2158–2170.
Fitton, J.G., Saunders, A.D., Norry, M.J., Hardarson, B.S., Taylor, R.N., 1997. Thermal and chemical structure of the Iceland plume. Earth and Planetary Science Letters 153, 197–208.
Foley, S., 2008. A trace element perspective on Archean crust formation and on the presence or absence of Archean subduction. In: Condie, K.C., Pease, V. (Eds.), When did Plate Tectonics Begin on Planet Earth? . Geological Society of America Special Paper, 440, pp. 31–50.
Gao, J., Li, M.S., Xiao, X.C., Tang, Y.Q., He, G.Q., 1998. Paleozoic tectonic evolution of the Tianshan Orogen, northwestern China. Tectonophysics 287, 213–231.
Gao, J., Long, L., Klemd, R., Qian, Q., Liu, D., Xiong, X., Su, W., Liu, W., Wang, Y., Yang, F., 2009. Tectonic evolution of the South Tianshan orogen and adjacent regions, NW China: geochemical and age constraints of granitoid rocks. International Journal of Earth Sciences 98, 1221–1238.
Gao, J., Klemd, R., Qian, Q., Zhang, X., Li, J., Jiang, T., Yang, Y., 2011. The collision between the Yili and Tarim blocks of the Southwestern Altaids: geochemical and age constraints of a leucogranite dike crosscutting the HP-LT metamorphic belt in the Chinese Tianshan Orogen. Tectonophysics 499, 118–131.
Ghiorso, M., Sack, R., 1995. Chemical mass transfer in magmatic processes IV. A revised and internally consistent thermodynamic model for the interpolation and extrapolation of liquid–solid equilibria in magmatic systems at elevated temperatures and pressures. Contributions to Mineralogy and Petrology 119, 197–212.
Griffin, W.L., Pearson, N.J., Belousova, E.A., Saeed, A., 2006. Comment: Hf-isotope heterogeneity in zircon 91500. Chemical Geology 233, 358–363.
Han, B.F., Guo, Z.J., Zhang, Z.C., Zheng, L., Chen, J.F., Song, B., 2010. Age, geochemistry, and tectonic implications of a Late Paleozoic stitching pluton in the North Tian Shan suture zone, western China. Geological Society of America Bulletin 122, 627–640.
Hirose, K., Kushiro, I., 1993. Partial melting of dry peridotites at high pressures: determination of compositions of melts segregated from peridotite using aggregates of diamond. Earth and Planetary Science Letters 114, 477–489.
Hu, A.Q., Wei, G.J., Jahn, B.M., Zhang, J.B., Deng, W.F., Chen, L.L., 2010. Formation of the 0.9 Ga Neoproterozoic granitoids in the Tianshan Orogen, NW China: constraints from the SHRIMP zircon age determination and its tectonic significance. Geochimica 39, 197–212.
Irvine, T.N., Baragar, W.R.A., 1971. A guide to the chemical classification of the common volcanic rocks. Canadian Journal of Earth Sciences 8, 523–548.
Jackson, S.E., Pearson, N.J., Griffin, W.L., Belousova, E.A., 2004. The application of laser ablation-inductively coupled plasma-mass spectrometry to in situ U–Pb zircon geochronology. Chemical Geology 211, 47–69.
Jahn, B.M., Wu, F.Y., Chen, B., 2000. Massive granitoid generation in Central Asia: Nd isotope evidence and implication for continental growth in the Phanerozoic. Episodes 23, 82–92.
Kelemen, P.B., Shimizu, N., Dunn, T., 1993. Relative depletion of niobium in some arc magmas and the continental crust: partitioning of K, Nb, La and Ce during melt/rock reaction in the upper mantle. Earth and Planetary Science Letters 120, 111–134.
Klein, M., Stosch, H.G., Seck, H.A., 1997. Partitioning of high field-strength and rare-earth elements between amphibole and quartz-dioritic to tonalitic melts: an experimental study. Chemical Geology 138, 257–271.
Li, X.-H., Li, Z.-X., Sinclair, J.A., Li, W.-X., Carter, G., 2006. Revisiting the "Yanbian Terrane": implications for Neoproterozoic tectonic evolution of the western Yangtze Block, South China. Precambrian Research 151, 14–30.
Liu, Y.S., Gao, S., Hu, Z.C., Gao, C.G., Zong, K.Q., Wang, D.B., 2010. Continental and oceanic crust recycling-induced melt–peridotite interactions in the Trans-North China Orogen: U–Pb dating, Hf isotopes and trace elements in zircons from mantle xenoliths. Journal of Petrology 51, 537–571.
Long, L., Gao, J., Klemd, R., Beier, C., Qian, Q., Zhang, X., Wang, J., Jiang, T., 2011. Geochemical and geochronological studies of granitoid rocks from the Western Tianshan Orogen: implications for continental growth in the southwestern Central Asian Orogenic Belt. Lithos 126, 321–340.
Ludwig, K.R., 2003. User's manual for Isoplot 3.00: a geochronological toolkit for Microsoft Excel. Berkeley Geochronology Center Special Publication 4, 1–70.
McKenzie, D., O'Nions, R.K., 1991. Partial melt distributions from inversion of rare earth element concentrations. Journal of Petrology 32, 1021–1091.
Middlemost, E.A.K., 1994. Naming materials in the magma/igneous rock system. Earth-Science Reviews 37, 215–224.
Patiño Douce, A.E., Beard, J.S., 1995. Dehydration-melting of biotite gneiss and quartz amphibolite from 3 to 15 kbar. Journal of Petrology 36, 707–738.
Pearce, J.A., Peate, D.W., 1995. Tectonic implications of the composition of volcanic arc magmas. Annual Review of Earth and Planetary Sciences 23, 251–285.
Pearce, J.A., Harris, N.B.W., Tindle, A.G., 1984. Trace element discrimination diagrams for the tectonic interpretation of granitic rocks. Journal of Petrology 25, 956–983.
Peccerillo, A., Taylor, S.R., 1976. Geochemistry of Eocene calc-alkaline volcanic rocks from the Kastamonu area, Northern Turkey. Contributions to Mineralogy and Petrology 58, 63–81.
Rapp, R.P., 1995. Amphibole-out phase boundary in partially melted metabasalt, its control over liquid fraction and composition, and source permeability. Journal of Geophysical Research: Solid Earth 100, 15601–15610.
Rapp, R.P., Watson, E.B., 1995. Dehydration melting of metabasalt at 8–32 kbar: implications for continental growth and crust–mantle recycling. Journal of Petrology 36, 891–931.
Rapp, R.P., Shimizu, N., Norman, M.D., Applegate, G.S., 1999. Reaction between slab-derived melts and peridotite in the mantle wedge: experimental constraints at 3.8 GPa. Chemical Geology 160, 335–356.
Rudnick, R.L., 1995. Making continental crust. Nature 378, 573–578.
Rudnick, R.L., Gao, S., 2003. The composition of the continental crust. In: Rudnick, R.L. (Ed.), The Crust. Elsevier—Pergamon, Oxford, pp. 1–64.
Said, N., Kerrich, R., 2010. Magnesian dyke suites of the 2.7 Ga Kambalda sequence, Western Australia: evidence for coeval melting of plume asthenosphere and metasomatised lithospheric mantle. Precambrian Research 180, 183–203.
Seltmann, R., Konopelko, D., Biske, G., Divaev, F., Sergeev, S., 2011. Hercynian post-collisional magmatism in the context of Paleozoic magmatic evolution of the Tien Shan orogenic belt. Journal of Asian Earth Sciences 42, 821–838.
Shaw, D.M., 1970. Trace element fractionation during anatexis. Geochimica et Cosmochimica Acta 34, 237–243.
Sisson, T.W., Ratajeski, K., Hankins, W.B., Glazner, A.F., 2005. Voluminous granitic magmas from common basaltic sources. Contributions to Mineralogy and Petrology 148, 635–661.
Smith, P.M., Asimow, P.D., 2005. Adiabat_1ph: a new public front-end to the MELTS, pMELTS, and pHMELTS models. Geochemistry, Geophysics, Geosystems 6, Q02004. http://dx.doi.org/10.1029/2004GC000816.
Sun, S.S., McDonough, W.F., 1989. Chemical and isotopic systematics of oceanic basalts: implications for mantle composition and processes. In: Saunders, A.D., Norry, M.J.

(Eds.), Magmatism in the Ocean Basins. Geological Society London Special Publications, pp. 313–345.
Takahashi, E., Kushiro, I., 1983. Melting of a dry peridotite at high pressures and basalt magma genesis. American Mineralogist 68, 859–879.
Tang, G.J., Wang, Q., Wyman, D.A., Sun, M., Li, Z.X., Zhao, Z.H., Sun, W.D., Jia, X.H., Jiang, Z.Q., 2010. Geochronology and geochemistry of Late Paleozoic magmatic rocks in the Lamasu–Dabate area, northwestern Tianshan (west China): evidence for a tectonic transition from arc to post-collisional setting. Lithos 119, 393–411.
Tang, G.J., Wang, Q., Wyman, D.A., Li, Z.X., Xu, Y.G., Zhao, Z.H., 2012a. Metasomatized lithosphere–asthenosphere interaction during slab roll-back: evidence from Late Carboniferous gabbros in the Luotuogou area, Central Tianshan. Lithos 155, 67–80.
Tang, G.J., Wang, Q., Wyman, D.A., Li, Z.X., Zhao, Z.H., Yang, Y.H., 2012b. Late Carboniferous high $\varepsilon_{Nd}(t)$–$\varepsilon_{Hf}(t)$ granitoids, enclaves and dikes in western Junggar, NW China: ridge-subduction-related magmatism and crustal growth. Lithos 140–141, 86–102.
Thirlwall, M.F., UPTON, B.G.J., Jenkins, C., 1994. Interaction between continental lithosphere and the Iceland plume—Sr–Nd–Pb isotope geochemistry of tertiary basalts, NE Greenland. Journal of Petrology 35, 839–879.
Tiepolo, M., Tribuzio, R., 2008. Petrology and U–Pb zircon geochronology of amphibole-rich cumulates with sanukitic affinity from husky ridge (Northern Victoria Land, Antarctica): insights into the role of amphibole in the petrogenesis of subduction-related magmas. Journal of Petrology 49, 937–970.
Tiepolo, M., Zanetti, A., Oberti, R., Brumm, R., Foley, S., Vannucci, R., 2003. Trace-element partitioning between synthetic potassic-richterites and silicate melts, and contrasts with the partitioning behaviour of pargasites and kaersutites. European Journal of Mineralogy 15, 329–340.
Wang, Q., Wyman, D.A., Zhao, Z.H., Xu, J.F., Bai, Z.H., Xiong, X.L., Dai, T.M., Li, C.F., Chu, Z.Y., 2007. Petrogenesis of carboniferous adakites and Nb-enriched arc basalts in the Alataw area, northern Tianshan Range (western China): implications for Phanerozoic crustal growth in the Central Asia orogenic belt. Chemical Geology 236, 42–64.
Wei, X., Xu, Y.G., Feng, Y.X., Zhao, J.X., 2014. Plume–lithosphere interaction in the generation of the Tarim large igneous province, NW china: geochronological and geochemical constraints. American Journal of Science 314, 314–356.
Wiedenbeck, M., AllÉ, P., Corfu, F., Griffin, W., Meier, M., Oberli, F., Quadt, A.V., Roddick, J., Spiegel, W., 1995. Three natural zircon standards for U–Th–Pb, Lu–Hf, trace element and REE analyses. Geostandards Newsletter 19, 1–23.
Windley, B.F., Allen, M.B., Zhang, C., Zhao, Z.Y., Wang, G.R., 1990. Paleozoic accretion and Cenozoic redeformation of the Chinese Tien Shan Range, Central Asia. Geology 18, 128–131.
Windley, B.F., Alexeiev, D., Xiao, W., Kroner, A., Badarch, G., 2007. Tectonic models for accretion of the Central Asian Orogenic Belt. Journal of the Geological Society, London 164, 31–47.
Wood, D.A., 1980. The application of a Th–Hf–Ta diagram to problems of tectonomagmatic classification and to establishing the nature of crustal contamination of basaltic lavas of the British Tertiary Volcanic Province. Earth and Planetary Science Letters 50, 11–30.
Workman, R.K., Hart, S.R., 2005. Major and trace element composition of the depleted MORB mantle (DMM). Earth and Planetary Science Letters 231, 53–72.
Wu, F.Y., Yang, Y.H., Xie, L.W., Yang, J.H., Xu, P., 2006. Hf isotopic compositions of the standard zircons and baddeleyites used in U–Pb geochronology. Chemical Geology 234, 105–126.
Xia, L.Q., Xu, X.Y., Xia, Z.C., Li, X.M., Ma, Z.P., Wang, L.S., 2004. Petrogenesis of Carboniferous rift-related volcanic rocks in the Tianshan, northwestern China. Geological Society of America Bulletin 116, 419–433.
Xia, L.Q., Xia, Z.C., Xu, X.Y., Li, X.M., Ma, Z.P., 2008. Relative contributions of crust and mantle to the generation of the Tianshan Carboniferous rift-related basic lavas, northwestern China. Journal of Asian Earth Sciences 31, 357–378.
Xiao, W.J., Zhang, L.C., Qin, K.Z., Sun, S., Li, J.L., 2004. Paleozoic accretionary and collisional tectonics of the eastern Tianshan (China): implications for the continental growth of central Asia. American Journal of Science 304, 370–395.
Xiao, W.J., Han, C.M., Yuan, C., Sun, M., Lin, S.F., Chen, H.L., Li, Z.L., Li, J.L., Sun, S., 2008. Middle Cambrian to Permian subduction-related accretionary orogenesis of Northern Xinjiang, NW China: implications for the tectonic evolution of central Asia. Journal of Asian Earth Sciences 32, 102–117.
Xiao, W., Huang, B., Han, C., Sun, S., Li, J., 2010. A review of the western part of the Altaids: a key to understanding the architecture of accretionary orogens. Gondwana Research 18, 253–273.
Xiao, W., Windley, B.F., Allen, M.B., Han, C., 2013. Paleozoic multiple accretionary and collisional tectonics of the Chinese Tianshan orogenic collage. Gondwana Research 23, 1316–1341.
Xu, X.Y., Xia, L.Q., Ma, Z.P., Wang, Y.B., Xia, Z.C., Li, X.M., Wang, L.S., 2006. SHRIMP zircon U–Pb geochronology of the plagiogranites from Bayringou ophiolite in North Tianshan Mountains and the petrogenesis of the ophiolite. Acta Petrologica Sinica 22, 83–94 (in Chinese with English abstract).
Xu, Y.G., Lan, J.B., Yang, Q.J., Huang, X.L., Qiu, H.N., 2008. Eocene break-off of the Neo-Tethyan slab as inferred from intraplate-type mafic dykes in the Gaoligong orogenic belt, eastern Tibet. Chemical Geology 255, 439–453.
Yang, J.-H., Wu, F.-Y., Wilde, S.A., Liu, X.-M., 2007a. Petrogenesis of Late Triassic granitoids and their enclaves with implications for post-collisional lithospheric thinning of the Liaodong Peninsula, North China Craton. Chemical Geology 242, 155–175.
Yang, J.H., Sun, J.F., Chen, F.K., Wilde, S.A., Wu, F.Y., 2007b. Sources and petrogenesis of late triassic dolerite dikes in the Liaodong Peninsula: implications for post-collisional lithosphere thinning of the Eastern North China Craton. Journal of Petrology 48, 1973–1997.
Yin, J., Yuan, C., Sun, M., Long, X., Zhao, G., Wong, K.P., Geng, H., Cai, K., 2010. Late Carboniferous high-Mg dioritic dikes in Western Junggar, NW China: geochemical features, petrogenesis and tectonic implications. Gondwana Research 17, 145–152.
Yin, J., Long, X., Yuan, C., Sun, M., Zhao, G., Geng, H., 2013. A Late Carboniferous–Early Permian slab window in the West Junggar of NW China: geochronological and geochemical evidence from mafic to intermediate dikes. Lithos 175–176, 146–162.
Zhang, C.-L., Zou, H.-b., 2013. Comparison between the Permian mafic dykes in Tarim and the western part of Central Asian Orogenic Belt (CAOB), NW China: implications for two mantle domains of the Permian Tarim Large Igneous Province. Lithos 174, 15–27.
Zhao, Z.H., Xiong, X.L., Wang, Q., Wyman, D.A., Bao, Z.W., Bai, Z.H., Qiao, Y.L., 2008. Underplating-related adakites in Xinjiang Tianshan, China. Lithos 102, 374–391.
Zhou, M.F., Zhao, J.H., Jiang, C.Y., Gao, J.F., Wang, W., Yang, S.H., 2009. OIB-like, heterogeneous mantle sources of Permian basaltic magmatism in the western Tarim Basin, NW China: implications for a possible Permian large igneous province. Lithos 113, 583–594.
Zhu, Y.F., Guo, X., Song, B., Zang, L.F., Gu, L.B., 2009. Petrology, Sr–Nd–Hf isotopic geochemistry and zircon chronology of the Late Palaeozoic volcanic rocks in the southwestern Tianshan Mountains, Xinjiang, NW China. Journal of the Geological Society, London 166, 1085–1099.
Zhu, Z.M., Zhao, Z.H., Xiong, X.L., Han, J.W., 2010. Petrogeochemistry of late Paleozoic gabbroic rocks from Tekes County in West Tianshan Mountains. Acta Petrologica et Mineralogica 29, 675–690.